EBioMedicine 57 (2020) 102832

Contents lists available at ScienceDirect

EBioMedicine

journal homepage: www.elsevier.com/locate/ebiom

Research paper

Itaconate prevents abdominal aortic aneurysm formation through inhibiting inflammation via activation of Nrf2

Haoyu Song[a,b], Tong Xu[a], Xiaofei Feng[a], Yanxian Lai[a], Yang Yang[a], Hao Zheng[a], Xiang He[a], Guoquan Wei[a], Wangjun Liao[d], Yulin Liao[a], Lintao Zhong[a,c,*], Jianping Bin[a,b,*]

[a] Department of Cardiology, State Key Laboratory of Organ Failure Research, Nanfang Hospital, Southern Medical University, 1838 North Guangzhou Avenue, Guangzhou 510515, China
[b] Guangzhou Regenerative Medicine and Health Guangdong Laboratory, Guangzhou 510005, China
[c] Zhuhai People's Hospital (Zhuhai hospital affiliated with Jinan University), Zhuhai 519000, China
[d] Department of Oncology, Nanfang Hospital, Southern Medical University, Guangzhou 510515, China

ARTICLE INFO

Article History:
Received 13 November 2019
Revised 23 May 2020
Accepted 27 May 2020
Available online 20 June 2020

Keywords:
Itaconate
Abdominal aortic aneurysm
Angiotensin II
Inflammation

ABSTRACT

Background: Identifying effective drugs to suppress vascular inflammation is a promising strategy to delay the progression of abdominal aortic aneurysm (AAA). Itaconate has a vital role in regulating inflammatory activation in various inflammatory diseases. However, the role of itaconate in the progression of AAA is unknown. In this study, we explored the inhibitory effect of itaconate on AAA formation and its underlying mechanisms.

Methods: Quantitative PCR, western blotting and immunohistochemistry were used to determine Irg1 and downstream Nrf2 expression in human and mouse AAA samples. Liquid chromatograph-mass spectrometry (LC-MS) analysis was performed to measure the abundance of itaconate. OI treatment and Irg1 knockdown were performed to study the role of OI in AAA formation. Nrf2 intervention in vivo was performed to detect the critical role of Nrf2 in the beneficial effect of OI on AAA.

Findings: We found that itaconate suppressed the formation of angiotensin II (Ang II)-induced AAA in apolipoprotein E-deficient ($Apoe^{-/-}$) mice, while Irg1 deficiency exerted the opposite effect. Mechanistically, itaconate inhibited vascular inflammation by enabling Nrf2 to function as a transcriptional repressor of downstream inflammatory genes via alkylation of Keap1. Moreover, Nrf2 deficiency significantly aggravated inflammatory factor expression and promoted AAA formation. In addition, Keap1 overexpression significantly promoted Ang II-induced AAA formation, which was inhibited by itaconate.

Interpretation: Itaconate inhibited AAA formation by suppressing vascular inflammation, and therapeutic approaches to increase itaconate are potentially beneficial for preventing AAA formation.

Funding: National Natural Science Foundations of China and Guangzhou regenerative medicine and Health Laboratory of Guangdong.

1. Introduction

Abdominal aortic aneurysm is a chronic inflammatory disease. An accumulating body of evidence has indicated that regulating the expression of inflammation-related genes is a promising strategy to control the progression of abdominal aortic aneurysm (AAA) [1–3]. In various studies, knockout/in of genes or transfection of viruses such as lentivirus (LV), adeno-associated virus (AAV) and adenovirus (ADV) have been used to regulate gene expression. These gene editing tools are widely used to regulate the expression of inflammation-related genes to inhibit AAA formation by reducing the activation of inflammatory signaling pathways, such as knockout of interleukin-1beta (IL-1β) [4], knock-in of SIRT1 [5], LV-mediated microRNA 24 overexpression [6] or AAV9-mediated H19 suppression [7]. In addition, studies have suggested that injection of monoclonal antibodies against inflammatory factor receptors [8], such as interleukin-6 (IL-6) receptors [9], inhibits the formation and progression of aneurysms. However, these gene editing tools and monoclonal antibodies are

Abbreviations: AAA, abdominal aortic aneurysm; Ang II, angiotensin II; OI, 4-octyl itaconate; Irg1, immune responsive gene 1; Nrf2, nuclear factor (erythroid-derived 2)-like 2; MCP1, monocyte chemotactic protein-1; MMP, matrix metalloproteinase; siRNA, small-interfering RNA; IL-6, interleukin-6; IL-1β, interleukin-1β; IFN-γ, interferon-γ; Keap1, Kelch-like ECH-associated protein 1

* Corresponding authors at: Department of Cardiology, State Key Laboratory of Organ Failure Research, Nanfang Hospital, Southern Medical University, 1838 North Guangzhou Avenue, Guangzhou 510515, China.
E-mail addresses: 598938020@qq.com (L. Zhong), jianpingbin@126.com (J. Bin).

https://doi.org/10.1016/j.ebiom.2020.102832

Research in context

Evidence before this study

A previous study showed that upon exposure to inflammatory stimuli, macrophages underwent metabolic signaling to produce itaconate, which markedly decreased the production of proinflammatory mediators in activated macrophages. In vitro experiments enhancing Irg1 expression showed reduced release of tumor necrosis factor-α (TNF-α) and interleukin-6 (IL-6) from activated macrophages, while knockout of Irg1 aggravated the inflammatory response. More importantly, in vivo experiments have shown anti-inflammatory effects when mice were administered itaconate during psoriasis, sepsis and ischemia-reperfusion injury.

Added value of this study

We found that itaconate suppressed the formation of angiotensin II (Ang II)-induced AAA in apolipoprotein E-deficient ($Apoe^{-/-}$) mice, while Irg1 deficiency exerted the opposite effects. Mechanistically, itaconate inhibited vascular inflammation by enabling Nrf2 to function as a transcriptional repressor of downstream inflammatory genes via alkylation of Keap1. Moreover, Nrf2 deficiency significantly aggravated inflammatory factor expression and promoted AAA formation. In addition, Keap1 overexpression significantly promoted Ang II-induced AAA formation, which was inhibited by itaconate.

Implication of all available evidence

In summary, our work showed that Irg1/itaconate protected against AAA formation by promoting the activation of Nrf2, which suppressed AAA formation by inhibiting the expression of downstream inflammatory genes. Our findings suggest the potential of Irg1/itaconate to serve as a novel and inexpensive therapeutic target for AAA.

very expensive, and long-term injection of monoclonal antibodies can lead to drug resistance and diminished efficacy. In addition, there are ethical issues involved in gene editing tools used in clinical treatment.

Recently, studies have shown that endogenous metabolites play a key role in the progression of various pathological processes, such as alcohol-induced liver injury [10], cardiac hypertrophy [11–14] and atherosclerosis [15,16]. This kind of natural chemical compound is relatively inexpensive and easy to synthesize in large quantities. These characteristics of metabolites have prompted the implementation of clinical trials of some metabolite-derived drugs in patients with cardiovascular diseases [17,18] and Alzheimer's disease [19]. The findings of these studies indicate that metabolites have the potential to be novel and inexpensive treatment options for AAA. To develop this potential, we need to identify metabolites that can be used to treat aortic aneurysms and demonstrate their role in AAA models. A recent study showed that upon exposure to inflammatory stimuli, macrophages underwent metabolic signaling to produce high levels of cellular metabolites such as itaconate, which is produced by the mitochondria-associated enzyme immune responsive gene 1 (Irg1), resulting in a marked decrease in the production of proinflammatory mediators in activated macrophages [20]. More importantly, in vitro experiments enhancing Irg1 expression showed reduced release of tumor necrosis factor-α (TNF-α) and IL-6 from activated macrophages, while knockout of Irg1 aggravated the inflammatory response [20]. In vivo experiments have shown anti-inflammatory effects when mice are administered itaconate during psoriasis [21], sepsis [22] and ischemia-reperfusion injury [20]. Interestingly, our preliminary results showed an increasing level of itaconate in aortic aneurysm specimens. These clues suggest that itaconate has potential in the treatment of inflammatory diseases. Given these findings, we hypothesized that itaconate inhibits AAA formation by reducing vascular inflammation.

Consistent with this hypothesis, we confirmed that itaconate/Irg1 protects against AAA formation. We found that exogenous addition of itaconate significantly reduced the vascular inflammation and aortic aneurysm formation rate. Then, we explored the underlying mechanism by which itaconate regulates vascular inflammation. We revealed that itaconate inhibited vascular inflammation by activating nuclear factor (erythroid-derived 2)-like 2 (Nrf2) to inhibit the expression of downstream inflammatory genes via alkylation of Kelch-like ECH-associated protein 1 (Keap1). Furthermore, we showed that Nrf2 acts as an intermediary in itaconate inhibition of AAA formation. We found that knockdown of Nrf2 promoted the progression of aortic aneurysm and inhibited the protective effect of itaconate on aortic aneurysm.

2. Materials and methods

The data that support the findings of this study are available from the corresponding author upon reasonable request.

2.1. Human aortic samples

Human AAA samples were obtained from patients undergoing open surgical repair according to protocols approved by the Research Ethics Committees of Nanfang Hospital (ethical approval number: NFEC-2019-086). Adjacent nonaneurysmal aortic segments were trimmed from the same patients and used as controls. All procedures complied with the principles of the Declaration of Helsinki. Each subject signed the informed consent for collection of aortic samples for research purposes prior to inclusion in this study (patient clinical information is available in Supplemental Table I).

2.2. Experimental animals

Ten- to 12-week-old male C57BL/6J mice with normal lipid metabolism and 10- to 12-week-old male $Apoe^{-/-}$ mice generated on the C57BL/6J background were purchased from the Laboratory Animal Center of Southern Medical University. All animal protocols were approved by the Institutional Animal Care and Use Committee at Southern Medical University. All animals were fed a normal chow diet and water and housed at a constant temperature of 22°C and 60%–65% humidity with a 12-h dark/light cycle in pathogen-free conditions. The care and experimental procedures of animals were in accordance with the Guidelines for the Care and Use of Laboratory Animals (NIH Publication, 8th Edition, 2011).

2.3. Ang II-induced AAA models

For establishment of the Ang II-induced AAA model, 10- to 12-week-old male C57BL/6J mice or $Apoe^{-/-}$ mice were injected with Ang II or saline as described previously [7]. In brief, mice were anesthetized by intraperitoneal injection of a mixture of xylazine (5 mg/kg) and ketamine (100 mg/kg). Adequate anesthesia was confirmed by the disappearance of pedal withdrawal reflex. Then, a mini osmotic pump (Alzet, Model 2004, DURECT Corporation, Cupertino, CA) loaded with Ang II (A9525; Sigma, St. Louis, MO) or saline was implanted into the subcutaneous space through a small incision in the dorsum of the neck. The injection was performed at a rate of 1 μg/kg/min. After 28 days, the mice were euthanized by an overdose of pentobarbital (150 mg/kg, i.p.), and the aortas were harvested for further morphological and histological analyses.

2.4. Pharmacologic intervention

For the preventive intervention study, we treated AAA model mice with an intraperitoneal injection of 4-octyl itaconate (OI, 50 mg/kg; 6662; Tocris Bioscience, UK) dissolved in 40% cyclodextrin (C4767; Sigma, Saint Louis, USA) in PBS three days before the Ang II injection and daily thereafter during the whole Ang II injection period. For comparison, another group of mice was administered 40% cyclodextrin as vehicle in parallel. OI or vehicle was also infused to mice using a mini osmotic pump at a rate of 35 μg/kg/min. The OI/vehicle pump and Ang II pump were implanted into mice simultaneously for 28 days.

2.5. Ultrasonic imaging

Ultrasonic B-mode images of the abdominal aortas were obtained in mice anesthetized with 2% isoflurane using a Vevo 2100 Imaging System (Visual Sonics, ON, Canada) equipped with a 40-MHz probe. Ultrasound was performed one day before model establishment as baseline and then measured on the 14th day and 28th day. The maximum aortic lumen diameters were measured (corresponding to cardiac systole) three times by a blinded investigator on the long axis of the suprarenal abdominal aorta. Data for the maximal aortic lumen diameter are shown for individual animals.

2.6. Aneurysm quantification

Mouse aortas were isolated at euthanasia after undergoing left ventricular puncture and phosphate-buffered saline (PBS) perfusion at physiological pressure. Necropsies were performed if the mice died during the experiment. After the periadventitial tissue was decorticated, the aortas were photographed using a digital camera.

The suprarenal abdominal aorta was defined as the part between the last pair of intercostal arteries and the right renal branch. The outer diameter of the maximal dilated portion of the suprarenal aorta was measured as the maximal aortic diameter using Image-Pro Plus software (Media Cybernetics) according to the aorta digital images. The ruptured aortas were excluded from the measurement of maximal aortic diameter. Aneurysm formation was identified as an increase in the outer width of the suprarenal aorta by at least 50% or greater compared with that in saline-treated mice as described in previous research [23]. Measurements were performed at least three times by two coworkers blinded to the group information before analysis.

2.7. Itaconate detection

Detection, identification and quantification of itaconate in the mouse aorta were performed as described [20]. Briefly, 50 mg of one sample was homogenized with 1000 μl of ice-cold methanol/water (70%, v/v) at 30 Hz for 3 min and centrifuged at 12,000 rpm at 4°C for 10 min. The collected supernatant was analyzed using an LC-ESI-MS/MS system (UPLC, Shim-pack UFLC SHIMADZU CBM A system; MS, QTRAP®6500+System). The analytical conditions were as follows: UPLC: column, Waters ACQUITY UPLC HSS T3 C18 (1.8 μm, 2.1 mm $\times$ 100 mm); column temperature, 40°C; flow rate, 0.4 mL/min; injection volume, 2 μL; solvent system, water (0.04% acetic acid): acetonitrile (0.04% acetic acid); gradient program, 95:5 V/V at 0 min, 5:95 V/V at 11.0 min, 5:95 V/V at 12.0 min, 95:5 V/V at 12.1 min, 95:5 V/V at 14.0 min. LIT and triple quadrupole (QQQ) scans were acquired on a triple quadrupole-linear ion trap mass spectrometer (QTRAP), QTRAP® 6500+ LC-MS/MS System, equipped with an ESI Turbo Ion-Spray interface, operating in positive and negative ion mode and controlled by Analyst 1.6.3 software (Sciex). The ESI source operation parameters were as follows: source temperature 500°C; ion spray voltage (IS) 5500 V (positive), -4500 V (negative); ion source gas I (GSI), gas II (GSII), and curtain gas (CUR) were set at 55, 60, and 25.0 psi, respectively; and the collision gas (CAD) was high. Instrument tuning and mass calibration were performed with 10 and 100 μmol/L polypropylene glycol solutions in QQQ and LIT modes, respectively. A specific set of MRM transitions was monitored for each period according to the metabolites eluted within this period.

2.8. Blood pressure measurement

Systolic blood pressure of the mice was measured noninvasively using tail-cuff plethysmography (BP-2010 series, Softron, Tokyo) as described in a previous study [24]. This measurement was initiated one day before pump implantation and continued weekly throughout the injection process.

2.9. Histological analysis and elastin degradation

Aortic samples isolated from the mice were fixed with 4% paraformaldehyde for 24 h and embedded in paraffin. Serial sections (5 μm each) were created at intervals of approximately 500 μm. At least 10 sections were observed in each animal. Paraffin sections were further used for elastin van Gieson staining or immunohistochemistry.

For semiquantitative analysis of elastin degradation, we referred to a standard for the elastin degradation score as described in a previous study [5]: score 1, no degradation; score 2, mild elastin degradation; score 3, severe elastin degradation; score 4, aortic rupture. The elastin degradation scores are presented as the medians and quartiles.

2.10. RNA extraction and quantitative real-time polymerase chain reaction (qPCR)

Total RNA from mouse abdominal aortic tissues or cultured cells was extracted using TRIzol reagent (Invitrogen) after homogenization in accordance with the manufacturer's instructions. Isolated RNA was reverse-transcribed to cDNA using reverse transcriptase (TaKaRa Biotechnology, Dalian, China). qPCR was performed with Light Cycler 480 II equipment (Roche Diagnostics, Basel, Switzerland) using a SYBR Green RT-PCR Kit (TaKaRa Biotechnology, Dalian, China). The relative mRNA expression was normalized to glyceraldehyde-3-phosphate dehydrogenase (GAPDH) and assessed according to the 2-$\Delta\Delta$Ct method.

The primers used were synthesized by Saicheng Biotech (Guangzhou, China), and the primer sequences are available in Supplemental Table II.

2.11. Immunohistochemistry staining

Immunohistochemistry staining was performed as previously described [25]. Paraffin-embedded sections were deparaffinized and rehydrated sequentially in xylene, 100% ethanol, 90% ethanol, 70% ethanol, and distilled water. Then, the sections were autoclaved in 10 mmol/L sodium citrate buffer (pH 6.0) for antigen retrieval at 121°C for 15 min and treated with 3% hydrogen peroxide to quench endogenous peroxidase activity at room temperature for 10 min. The nonspecific binding sites were blocked with 2% bovine serum albumin (BSA) at room temperature for 1 h. Next, aortic sections were incubated with primary antibodies (in 1% BSA) at 4°C overnight and secondary antibodies (in 1% BSA) at 37°C for 30 min. Finally, the sections were stained with diaminobenzidine and counterstained with hematoxylin.

The primary antibodies used were anti-Nrf2, anti-MMP2, anti-MMP9, anti-MAC2, anti-MCP1, and anti-IL-6 with the corresponding dilution. For the negative controls, the primary antibody was replaced with rabbit IgG. Information about the antibodies is available in Supplemental Table III.

Immunohistochemistry staining of Irg1, MAC2, MCP1, MMP2, MMP9 and IL-6 was analyzed by calculating the integration optical density value of positive staining using Image-Pro Plus software (Media Cybernetics). A minimum of three microscopic fields of stained slides were randomly observed by two independent researchers who were unaware of the group information.

2.12. Cell culture and treatments

The mouse macrophage cell (Raw 264.7) line, mouse aortic vascular smooth muscle cell (VSMC) line and mouse endothelial cell (EC) line were purchased from Guangzhou Geneseed Biotech, Ltd., and maintained in DMEM (Gibco BRL) supplemented with 10% fetal bovine serum (FBS, Gibco BRL), 100 IU/mL penicillin (Gibco BRL), and 100 μg/mL streptomycin (Gibco BRL) at 37°C in a humidified atmosphere containing 5% CO_2.

For the isolation of inflammatory peritoneal macrophages, the mice were intraperitoneally injected with 1 mL of 4% thioglycolate (TG). Cells were collected through peritoneal lavage at 4 days. Macrophages were purified by seeding collected cells in culture dishes with 10% fetal bovine serum and 1% penicillin/streptomycin-containing RPMI 1640 medium (Gibco BRL) for 1 h at 37°C. Then, nonadherent cells were discarded by washing with PBS three times, and adherent macrophages were cultured for further experiments [6].

For the experiments, cells were seeded at a concentration of 10^6 cells per mL in various culture dishes and treated separately.

2.13. Small-interfering RNA (siRNA) transfection and RNA interference

The siRNA sequences against Irg1 and Nrf2 and the overexpression plasmids pEnter-Nrf2 and pEnter-Keap1 were synthesized by Vigene Bioscience (Jinan, Shandong, China). Raw 264.7 cells were seeded into 6-well plates and grown to a concentration of 10^6 cells per mL. On the day of transfection, the media were replaced with DMEM without FBS or penicillin/streptomycin. For every target gene, two Eppendorf tubes with 250 μL of Opti-Minimum Essential Medium (Gibco BRL, Paisley, United Kingdom) were prepared. SiRNA (50 nM) or overexpression plasmid (4 μg) was seeded into one tube, and Lipofectamine 3000 (L3000015; Invitrogen) was seeded into another tube. Then, the solutions in the two tubes were mixed together and incubated at room temperature for 30 min before being added to each well. After a 6-h incubation, the medium was replaced with DMEM supplemented with FBS and penicillin/streptomycin. After 48 h of growth, the cells were treated as required. The Irg1 and Nrf2 siRNA sequences are shown in Supplemental Table V.

AAV2-containing GFP vectors for Irg1 depletion, Nrf2 depletion, and Nrf2 overexpression were generated [26]. In the in vivo experiments, mice were injected with the corresponding virus (1×10^{11} vector genomes) via the tail vein. After the mice were raised for 30 days, they were randomly grouped and treated with Ang II as mentioned previously.

2.14. Enzyme-linked immunosorbent assay (ELISA)

Cytokine IL-6 and IL-1β concentrations in the serum samples or cell supernatants were quantified using ELISAs as described in a previous study [27]. Mouse blood was recovered from the abdominal aortas into tubes containing citrate-phosphate-dextrose anticoagulant and centrifuged to collect the serum. A mouse IL-6 ELISA kit (P08505; CUSABIO, Wuhan, Hubei, China) and a mouse IL-1β ELISA kit (P10749; CUSABIO, Wuhan, Hubei, China) were used according to the manufacturer's protocols. Optical density values were measured at a wavelength of 450 nm in an ELISA plate reader (Spectra Max M5, Molecular Devices, California, United States).

2.15. Western blot analysis

Western blotting was performed as previously described [28,29]. Mouse aortic tissue or cellular proteins were extracted using radioimmunoprecipitation assay (RIPA) buffer (25 mM Tris−HCl pH 7.6, 150 mM NaCl, 1% NP-40, 1% sodium deoxycholate, and 0.1% SDS). Nuclear proteins were extracted via the nuclear extraction kit (Sigma, Shanghai, China). After homogenization and high-speed centrifugation, supernatant protein extracts were collected. Briefly, protein samples were electrophoresed on 10% SDS-PAGE running gels and transferred onto polyvinylidene fluoride (PVDF) membranes. Then, the membranes were blocked with 5% BSA in TBST at 37°C for 2 h and incubated with primary antibody at 4°C overnight. The primary antibodies used were anti-Irg1, anti-Nrf2, anti-Keap1, anti-MMP9, anti-MMP2, anti-MCP1, anti-β-actin, and anti-LaminB1 with the corresponding dilutions. Information about the antibodies is available in Supplemental Table VI.

Membranes were washed with TBST and incubated with a horseradish peroxidase-conjugated secondary antibody. Protein bands were detected by enhanced chemiluminescence (Advance, No. RPN2235; GE Healthcare Life Sciences). Western blots were replicated at least three times and quantified by ImageJ software (National Institutes of Health, Bethesda, MD). The intensity values were normalized to those of β-actin for total proteins and Lamin B1 for nuclear proteins.

2.16. Chromatin immunoprecipitation with quantitative PCR (ChIP-qPCR)

ChIP assays were performed using the Pierce™ Agarose ChIP Kit (26156; Thermo Fisher Scientific) according to the manufacturer's protocol. Briefly, the Raw 264.7 cells were fixed with 1% formaldehyde at room temperature for 30 min and quenched with 125 mM glycine for 5 min, followed by DNA fragmentation by sonication at 3 s/10 s 30 times. Subsequently, chromatin was immunoprecipitated with biotin-labeled anti-Nrf2 antibody. A positive control antibody (RNA polymerase II/RPII), a negative control normal human IgG, and GAPDH primers were used as controls. Purified chromatin was quantified by qRT-PCR using a SYBR Premix Ex Taq™ Kit (TaKaRa Biotechnology, Dalian, China) with the corresponding designed primers (primer sequences are available in Supplemental Table VII). Fold enrichment was quantified using qRT-PCR and calculated as a percentage of the input chromatin (% input).

2.17. Statistical analysis

Statistical analyses were performed using SPSS, version 20.0 (SPSS, Inc., Chicago, IL). For all continuous variables, a normal distribution test was performed. After confirmation of the variance equality between different groups, significant differences between two independent groups were analyzed using unpaired Student's t test, whereas significant differences between multiple groups were analyzed using one-way ANOVA with a post Bonferroni's multiple comparisons test. For variables with a non-normal distribution, a nonparametric Mann-Whitney U test for two independent groups was applied. The aortic incidence between the two groups was compared using Fisher's exact test. In this study, the elastin degradation scores are presented as medians and quartiles, and the remaining values are presented as the mean±SD. $P<0.05$ was considered statistically significant.

3. Results

3.1. Itaconate production is elevated in human and mouse AAA tissues

To test the hypothesis that itaconate is related to the pathogenesis of AAA, we first investigated the expression of Irg1, the gene

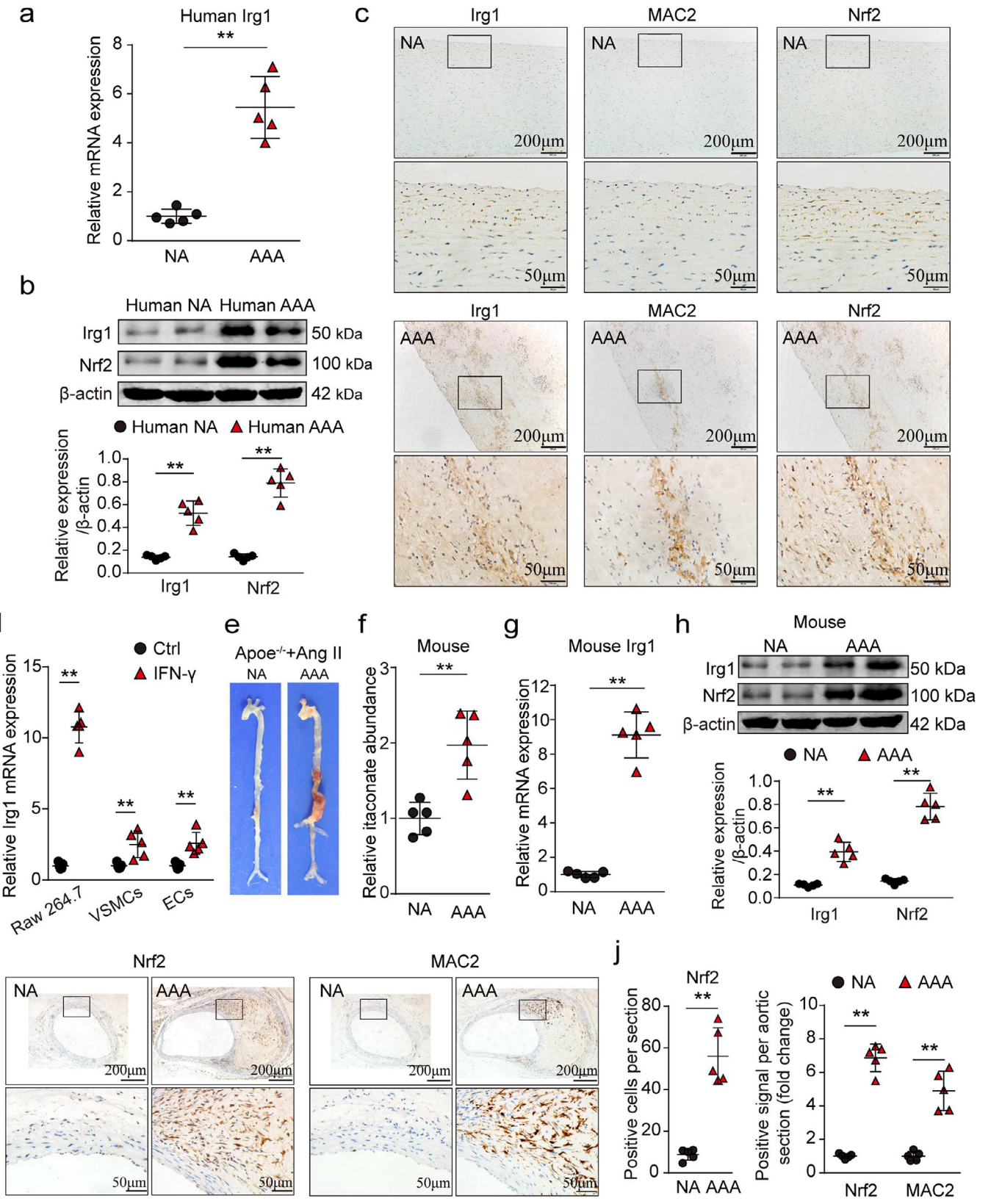

Fig. 1. Itaconate production is increased in human and mouse Ang II (angiotensin II)-induced AAA tissues. (a) PCR analysis of Irg1 in human abdominal aortic aneurysm (AAA) and adjacent nonaneurysmal aortic (NA) samples. $^{**}p<0.01$; n=5 per group (parametric paired t test). (b) Western blots (WBs) of the protein levels of Irg1 and Nrf2 in human AAA and NA samples. $^{**}p<0.01$; n=5 per group (parametric paired t test). (c) Representative immunohistochemical staining in serial sections showing the expression of Irg1, MAC2 and Nrf2 in human AAA and NA samples (scale bars=200 and 50 μm; n=5 per group). (d) PCR analysis of Irg1 in Raw 264.7 cells, vascular smooth muscle cells (VSMCs) and endothelial cells (ECs) after stimulation with or without IFN-γ (12 h). $^{**}p<0.01$; n=5 per group (parametric unpaired t test). (e) Representative photographs showing the macroscopic features of the aortas from Apoe$^{-/-}$ mice treated with Ang II or saline. (f) Relative itaconate abundance in AAA samples from Ang II-induced Apoe$^{-/-}$ mice and NA samples from saline-induced control Apoe$^{-/-}$ mice. $^{**}p<0.01$; n=5 per group (parametric unpaired t test). (g) PCR analysis of Irg1 in AAA samples from Ang II-induced Apoe$^{-/-}$ mice and NA samples from saline-

encoding the enzyme producing itaconate, in human AAA samples. Human AAA tissues and their control adjacent aortic sections without aneurysms were obtained from patients undergoing open surgery. Both qPCR and Western blotting showed that Irg1 expression was substantially higher in human AAA tissues than in the corresponding adjacent nonaneurysmal tissues ($p<0.01$, parametric unpaired t test, Fig. 1a and b). Immunohistochemical staining of Irg1, Nrf2 and MAC2 (a marker of macrophage) in serial sections showed that the upregulation of Irg1 and Nrf2 mainly occurred in macrophages, as the positive stained regions of Irg1 and Nrf2 coincide with those of MAC2 (Fig. 1c). Besides, we assessed Irg1 levels in macrophages, VSMCs and endothelial cells (ECs) as these three kinds of cells mediate inflammatory reactions in AAA [30,31]. Mouse Raw264.7 cells, VSMCs and ECs were cultured and stimulated with interferon-gamma (IFN-γ) to mimic the AAA environment. qPCR analyses showed the most significant upregulation of Irg1 mRNA in Raw264.7 cells ($p<0.01$ vs. Ctrl, parametric unpaired t test, Fig. 1d), suggesting that the Irg1/itaconate pathway is mainly increased in activated macrophages.

Currently, Ang II-induced mouse AAA formation in Apoe$^{-/-}$ mice has become the most widely used AAA model [32,33]. As previously described, we established an Ang II-induced mouse AAA model and its corresponding control by infusing Ang II or saline with a minipump for four weeks in male Apoe$^{-/-}$ mice. Macroscopic analysis showed aneurysm formation at 28 days in Ang II-infused mice but not in saline-infused control mice, indicating successful AAA model establishment (Fig. 1e). Metabolomic profiling of aortic samples from the two groups revealed that endogenous itaconate was highly accumulated in the Ang II-infused group ($p<0.01$, parametric unpaired t test, Fig. 1f). We next evaluated Irg1 and Nrf2 expression in the mice. Both qPCR and Western blotting indicated a significant increase in Irg1 and Nrf2 expression in Ang II-infused mice ($p<0.01$, parametric unpaired t test, Fig. 1g and h), which was consistent with the elevated itaconate abundance. Furthermore, immunohistochemical results confirmed the increased Nrf2 levels and infiltrating macrophages in the mouse aorta after Ang II infusion ($p<0.01$, parametric unpaired t test, Fig. 1i and j).

Collectively, these findings suggested that elevated itaconate production was involved in the process of AAA formation.

3.2. Itaconate treatment attenuates Ang II-induced AAA formation

To determine the role of itaconate in AAA formation, we first tested the effect of exogenous itaconate addition in the Ang II-induced mouse AAA model. A cell-permeable itaconate analogue, 4-octyl itaconate (OI) [34], was applied in our experiment. Apoe$^{-/-}$ mice were treated daily with OI or vehicle three days before Ang II infusion and thereafter for 28 days. After 28 days of chronic infusion of Ang II, experimental AAAs were induced (Fig. 2a). The systolic blood pressure after Ang II infusion did not differ between the two groups ($p>0.05$, parametric unpaired t test, Supplemental Fig. 1a). In the vehicle-treated group, 75.0% (27/36) of the mice exhibited AAA formation, while in the OI-treated group, only 36.0% (13/36) showed AAA formation ($p<0.01$, Fisher's exact test, Fig. 2b). Approximately 25.0% (9/36) of mice in the vehicle-treated group died because of aortic rupture, whereas only 8.3% (3/36) of mice in the OI-treated group died (Fig. 2c). The maximal abdominal aortic diameter was substantially lower in OI-treated mice than vehicle-treated mice ($p<0.01$, parametric unpaired t test, Fig. 2d). The elastin degradation scores for the abdominal aortas were significantly lower in the OI-treated group than in the vehicle-treated group ($p<0.01$, non-parametric ANOVA Kruskal-Wallis test with post Dunn's multiple comparisons test, Fig. 2e-f). Moreover, inflammatory cell infiltration as determined by MAC2 was decreased in the OI-treated group ($p<0.01$ vs. Vehicle, parametric unpaired t test, Fig. 2g-h).

Matrix metalloproteinase 9 (MMP9), MMP2 and monocyte chemoattractant protein-1 (MCP-1/CCL2) play critical roles in AAA initiation and progression [35,36]. As shown in the immunohistochemistry and Western blotting results, the aortas from OI-treated mice exhibited a significant decrease in the levels of MMP9, MMP2 and MCP1 compared with those of vehicle-treated control mice ($p<0.01$, parametric unpaired t test, Fig. 2i–l, Supplemental Fig. 2b–e). Furthermore, we investigated expression of the proinflammatory cytokines IL-6 and IL-1β after 28 days of Ang II infusion. In the OI-treated group, the aortic secretions of IL-6 and IL-1β were restrained ($p<0.01$ vs. Vehicle, parametric unpaired t test, Fig. 2m), suggesting the regulatory effect of OI on the inflammatory response.

To reduce stress injury by daily intraperitoneal injection, we also used mini osmotic pumps to infuse OI. Two minipumps separately loaded with OI/vehicle and Ang II were implanted into mice. During the infusion period, vascular ultrasound imaging showed progressively greater dilation and aneurysm formation on the 14th day and the 28th day in the abdominal aorta of OI treated mice compared with vehicle treated mice (Supplemental Fig. 2a). OI-treated mice also exhibited lower lumen diameters both on the 14th day and the 28th day (Supplemental Fig. 2b). Morphological and elastin staining analyses showed that OI infused by pumps also inhibited AAA formation in 28-day Ang II-infused mice (Supplemental Fig. 2c–g). These results further corroborated the protective effect of OI.

Taken together, these data indicated that itaconate treatment attenuated Ang II-induced AAA formation and regulated inflammation.

3.3. Reduction of endogenous itaconate promotes Ang II-induced AAA formation

We further investigated the role of endogenous itaconate in AAA formation. Irg1 is the only enzyme catalyzing itaconate synthesis [20]. To reduce the content of itaconate in vivo, we generated an AAV carrying siRNA against Irg1 to inhibit endogenous itaconate production. Four siRNA sequences against Irg1 were separately transfected into cultured Raw 264.7 cells. The interference effects were detected by qPCR (Supplemental Fig. 3a), and the most potent siRNA sequence was selected to package AAV serotype 2 (AAV2). To verify the transfection effect of the virus, we administered AAVs carrying Irg1 siRNA (Sh-Irg1 group) or scramble RNA (Scr-RNA group) to the mice via the tail vein. Aortic Irg1 expression was assessed serially on the 15th, 30th, 40th, 50th, and 60th days. Western blot analyses showed that significant Irg1 suppression began on the 15th day, peaked on the 30th day and continued until the 60th day (Supplemental Fig. 3b).

We then studied whether Irg1 knockdown influenced AAA development in vivo by examining the index in aortas mentioned above in Irg1 knockdown (Sh-Irg1) or control (Scr-RNA) C57/BL6J mice with Ang II infusion for 28 days. WB analyses showed that Irg1 was decreased in the Sh-Irg1 group compared with the Scr-RNA group ($p<0.01$, parametric unpaired t test, Supplemental Fig. 4a). Systolic blood pressure was not significantly different between the two groups ($p>0.05$, parametric unpaired t test, Supplemental Fig. 4b). The control C57/BL6J mice had a very low AAA incidence after Ang-II infusion, while Irg1 knockdown mice significantly enhanced AAA formation, as shown in macroscopic photographs (Fig. 3a). Four weeks of Ang II infusion caused a 47.2% (17/36) incidence of AAA in Sh-Irg1

induced control Apoe$^{-/-}$ mice. $^{**}p<0.01$; n=5 per group (parametric unpaired t test). (h) WB analysis of Irg1 and Nrf2 in mouse AAA and NA samples. $^{**}p<0.01$; n=5 per group (parametric unpaired t test). (i and j) Representative immunohistochemical staining and corresponding quantification of Nrf2 and MAC2 levels in mouse AAA and NA samples (scale bars=200 and 50 μm). $^{**}p<0.01$; n=5 per group (parametric unpaired t test).

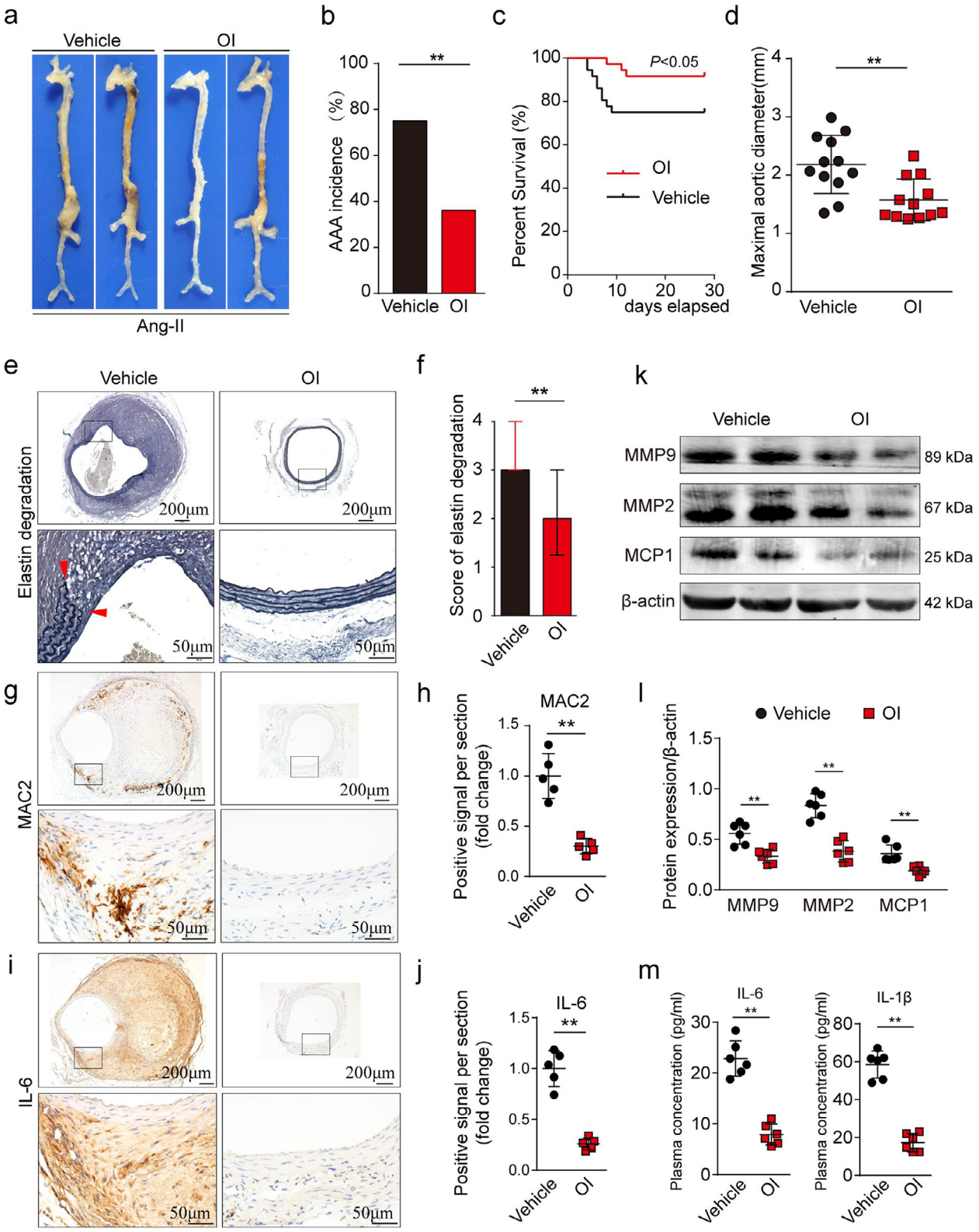

Fig. 2. Exogenous addition of the itaconate analogue 4-octyl itaconate (OI) attenuates Ang II-induced AAA formation in Apoe$^{-/-}$ mice. (a) Representative images of the macroscopic features of AAA in Ang II-infused Apoe$^{-/-}$ mice. (b) The incidence of Ang II-induced AAA in OI-treated Apoe$^{-/-}$ mice (n=36) compared with those in vehicle-treated Apoe$^{-/-}$ mice (n=36). $^{**}p<0.01$ (Fisher's exact test). The number of mice that developed AAA included deaths caused by abdominal aortic rupture. (c) The survival curve of Ang II-induced AAA in the two groups. $p<0.05$; n=36 per group (Log-rank (Mantel-Cox) test). (d) The maximal abdominal aortic diameter in Ang II−infused Apoe$^{-/-}$ mice. $^{**}p<0.01$; n=12 per group (parametric unpaired t test). (e and f) Representative staining with elastin and the elastin degradation score in the suprarenal aortas from Ang II-infused mice. The magnified photographs were taken at the location where the most severe elastin degradation occurred (scale bars=200 and 50 μm; magnified photographs). $^{**}p<0.01$; n=12 per group (non-parametric ANOVA Kruskal-Wallis test with post Dunn's multiple comparisons test). (g and h) Representative immunostaining and densitometric analysis of MAC2 in the suprarenal aortic walls (scale bars=200 and 50 μm). $^{**}p<0.01$; n=5 per group (parametric unpaired t test). (i and j) Representative immunostaining and densitometric analysis of IL-6 in the suprarenal aortic walls (scale bars, 200 and 50 μm). $^{**}p<0.01$; n=5 per group (parametric unpaired t test). (k and l) WB analysis of the protein levels of MMP2, MMP9, and MCP1 in the aortas from Ang II−infused Apoe$^{-/-}$ mice. $^{**}p<0.01$; n=6 per group (parametric unpaired t test). (m) Plasma IL-6 and IL-1β levels in the Ang II-treated Apoe$^{-/-}$ mice. $^{**}p<0.01$; n=6 per group (parametric unpaired t test).

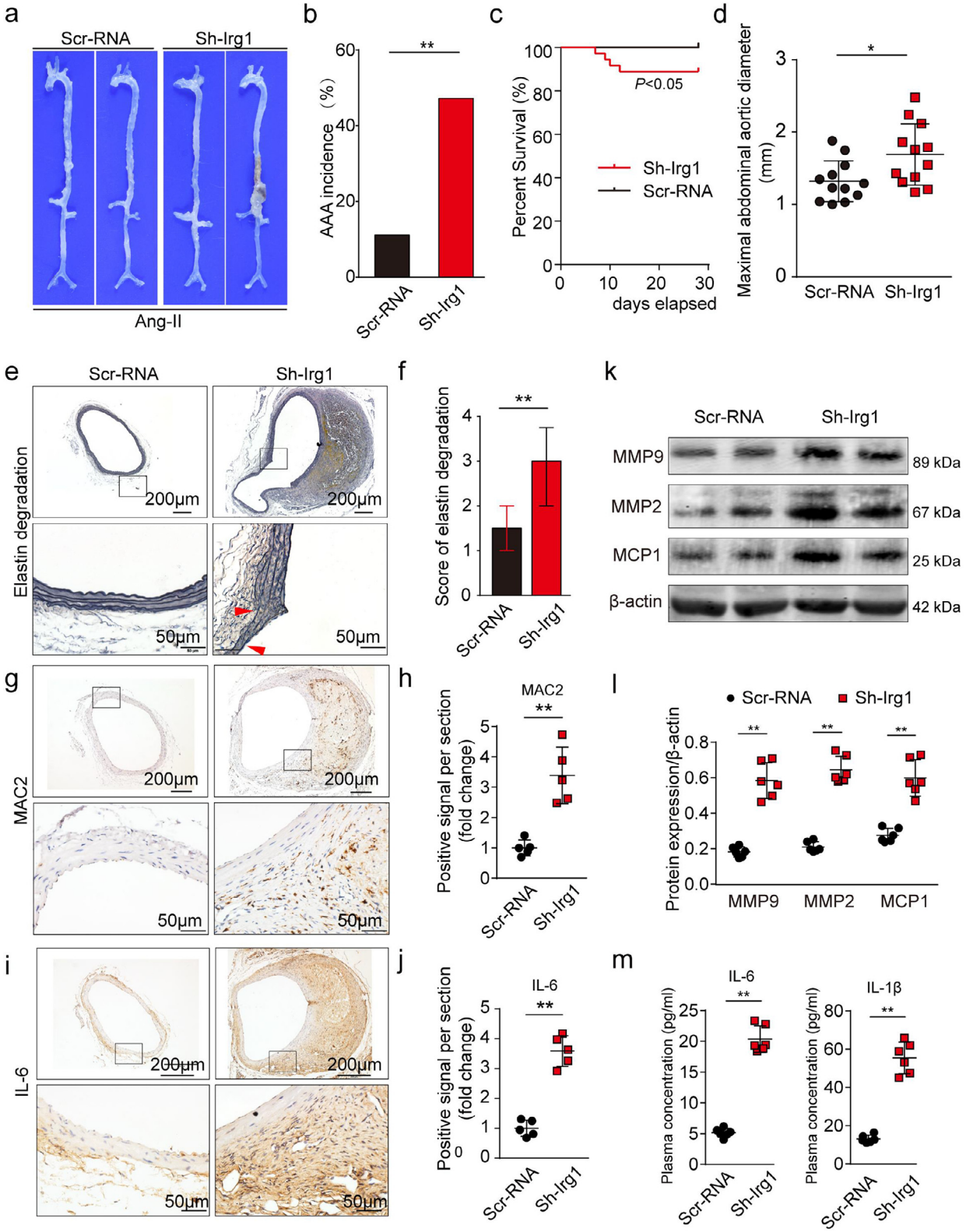

Fig. 3. Reduction of endogenous itaconate through knockdown of Irg1 promotes Ang II-induced AAA formation in C57BL/6J mice. (a) Representative images of the macroscopic features of AAA in the Ang II-infused C57BL/6J mice transfected with AAV carrying siRNA against Irg1 (Sh-Irg1) or scramble siRNA (Scr-RNA). (b) The incidence of Ang II-induced AAA in C57BL/6J mice. $^{**}p<0.01$; n=36 per group (Fisher's exact test). The number of mice that developed AAA included the deaths caused by abdominal aortic rupture. (c) The survival curve of Ang II-induced AAA in C57BL/6J mice in the two groups. $p<0.05$; n=36 per group (Log-rank (Mantel-Cox) test). (d) The maximal abdominal aortic diameter in Ang II−infused C57BL/6J mice. $^{*}p<0.05$; n=12 per group (parametric unpaired t test). (e and f) Representative staining with elastin and the elastin degradation score in the suprarenal aortas from Ang II−infused mice. The magnified photographs were taken at the location where the most severe elastin degradation occurred (scale bars=200 and 50 μm; magnified photographs). $^{**}p<0.01$; n=12 per group (non-parametric ANOVA Kruskal-Wallis test with post Dunn's multiple comparisons test). (g and h) Representative immunostaining and densitometric analysis of MAC2 in the suprarenal aortic walls (scale bars=200 and 50 μm). $^{**}p<0.01$; n=5 per group (parametric unpaired t test). (i and j) Representative immunostaining and densitometric analysis of IL-6 in the suprarenal aortic walls (scale bars=200 and 50 μm). $^{**}p<0.01$; n=5 per group (parametric unpaired t test). (k and l) WB analysis of the protein levels of MMP2, MMP9, and MCP1 in the aortas from Ang II−infused C57BL/6J mice. $^{**}p<0.01$; n=6 per group (parametric unpaired t test). (m) Plasma IL-6 and IL-1β levels in the Ang II-treated C57BL/6J mice. $^{**}p<0.01$; n=6 per group (parametric unpaired t test).

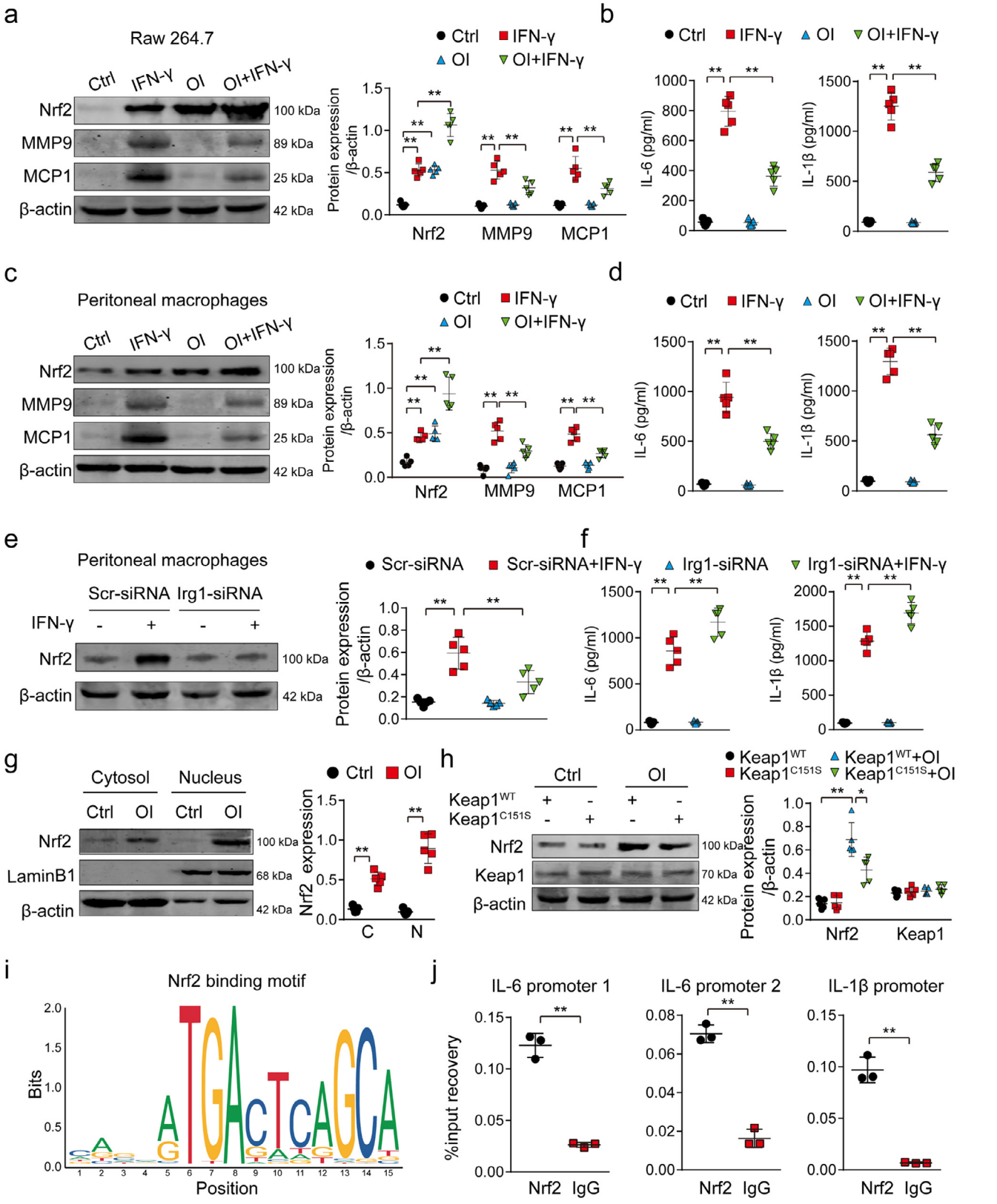

Fig. 4. Itaconate suppresses proinflammatory cytokines and matrix-degrading proteinases by activating Nrf2. (a) WB analysis of Nrf2, MMP9, MMP2 and MCP1 in the lysates of Raw 264.7 macrophages pretreated with vehicle or OI (12 h) and then stimulated with IFN-γ (24 h). $^{**}p<0.01$; n=5 per group (parametric one-way ANOVA with post Bonferroni's multiple comparisons test). (b) IL-1β and IL-6 levels secreted by Raw 264.7 macrophages treated as described in (a). $^{**}p<0.01$; n=5 per group (parametric one-way ANOVA with post Bonferroni's multiple comparisons test). (c) WB analysis of Nrf2, MMP9 and MCP1 in the lysates of peritoneal macrophages treated with OI or vehicle and then stimulated with IFN-γ (24 h). $^{**}p<0.01$; n=5 per group (parametric one-way ANOVA with post Bonferroni's multiple comparisons test). (d) IL-1β and IL-6 levels secreted by peritoneal macrophages treated with OI or vehicle and then stimulated with IFN-γ (24 h). $^{**}p<0.01$; n=5 per group (parametric one-way ANOVA with post Bonferroni's multiple comparisons test). (e) WB analysis of Nrf2 in the lysates of peritoneal macrophages after transfection with siRNA against Irg1 (Sh-Irg1) or scramble siRNA (Scr-RNA). $^{**}p<0.01$; n=5 per group (parametric one-way ANOVA with post Bonferroni's multiple comparisons test). (f) IL-1β and IL-6 levels secreted by peritoneal macrophages treated as described in (e). $^{**}p<0.01$; n=5 per group (parametric one-way ANOVA with post Bonferroni's multiple comparisons test). (g) WB analysis of Nrf2 in the total cytosol lysates and nuclear lysates of Raw 264.7 macrophages

group mice compared with only 11.1% (4/36) in the Scr-RNA group ($p<0.01$, Fisher's exact test, Fig. 3b). Approximately 11.1% (4/36) of Ang II–infused Sh-Irg1 group mice died because of aortic rupture, whereas no mice in the Scr-RNA group died (Fig. 3c). Compared with those of the Scr-RNA group, the maximal abdominal aortic diameter ($p<0.05$, parametric unpaired t test, Fig. 3d) and the elastin degradation score ($p<0.01$, non-parametric ANOVA Kruskal-Wallis test with post Dunn's multiple comparisons test, Fig. 3e and f) were substantially higher in the Sh-Irg1 group. However, there was no significant difference in the diameter of ascending aorta and thoracic aorta between the two groups (Supplemental Fig. 4c), suggesting that knockdown of Irg1 induced aortic dilation specifically in the abdominal aorta in Ang II-infused C57BL/6J mice. In addition, immunohistochemical staining showed that compared with the Scr-RNA group, the Sh-Irg1 group displayed significantly increased MAC2 ($p<0.01$, parametric unpaired t test, Fig. 3g-h) and IL-6 expression ($p<0.01$, parametric unpaired t test, Fig. 3i-h). Moreover, knockdown of Irg1 increased Ang II-induced MMP9, MMP2 and MCP1 expression, as shown by immunohistochemistry ($p<0.01$ vs. Scr-RNA, parametric unpaired t test, Supplemental Fig. 4d-g) and Western blotting ($p<0.01$, parametric unpaired t test, Fig. 3k-l). The cytokine levels of IL-6 and IL-1β were markedly elevated in the Sh-Irg1 group compared with the Scr-RNA group ($p<0.01$, parametric unpaired t test, Fig. 3m), suggesting that the lack of endogenous itaconate aggravated the inflammatory process.

The preceding data suggested that a lack of endogenous itaconate promoted Ang II-induced AAA formation and aggravated the inflammatory process.

3.4. Itaconate suppresses macrophage inflammatory responses by activating Nrf2

IFN-γ is elevated in serum and aneurysmal tissue during AAA formation and is implicated in AAA pathogenesis by activating macrophages and inducing MMPs production as reported in previous studies [37,38]. In macrophages, IFN-γ induces a strong upregulation of Irg1, which promotes itaconate production [39,40]. In our study, we used IFN-γ to stimulate Raw 264.7 macrophages to mimic the AAA environment and test the effect of exogenous itaconate addition on Nrf2 expression and the inflammatory response. In our experiment, we observed that IFN-γ promoted Nrf2 expression to some extent but increased MMP9 and MCP1 protein expression and inflammatory cytokine secretion ($p<0.01$ vs. Ctrl, parametric one-way ANOVA, Fig. 4a-b). Treatment with OI alone upregulated Nrf2 expression without inducing inflammatory responses. Pretreatment with OI and then stimulation with IFN-γ significantly enhanced Nrf2 levels and simultaneously decreased MMP9 and MCP1 protein expression ($p<0.01$ vs. IFN-γ, parametric one-way ANOVA, Fig. 4a). The IFN-γ-induced inflammatory cytokines IL-6 and IL-1β were also decreased by OI pretreatment ($p<0.01$ vs. IFN-γ, parametric one-way ANOVA, Fig. 4b). To further identify the role of itaconate, we assessed Nrf2 activation and inflammatory responses in the absence of endogenous itaconate. Raw 264.7 macrophages were transfected with siRNA against Irg1 (si-Irg1) or scramble RNA (scr-RNA) and then stimulated with IFN-γ. We found that knockdown of Irg1 blocked the IFN-γ-induced Nrf2 expression ($p<0.01$ vs. Scr-siRNA+IFN-γ, parametric one-way ANOVA, Supplemental Fig. 5a-b). Irg1 knockdown macrophages produced increased IL-6 and IL-1β levels after IFN-γ stimulation ($p<0.01$ vs. Scr-siRNA+IFN-γ, parametric one-way ANOVA, Supplemental Fig. 5c).

Thioglycolate (TG)-induced peritoneal macrophages are bone marrow–derived inflammatory cells that produce proinflammatory cytokines, which are considered to show the behaviors of infiltrating macrophages in AAA [41]. We then extracted TG-elicited mouse peritoneal macrophages from 10- to 12-week-old male C57BL/6J mice and performed similar experiments to further validate our conclusion. OI pretreatment enhanced Nrf2 levels and reduced the MMP9 and MCP1 protein expression and inflammatory cytokine secretion induced by IFN-γ ($p<0.01$ vs. IFN-γ, parametric one-way ANOVA, Fig. 4c and d). Conversely, knockdown of Irg1 by siRNA against Irg1 blocked IFN-γ-induced Nrf2 expression and increased inflammatory cytokine secretion ($p<0.01$ vs. Scr-siRNA+IFN-γ, parametric one-way ANOVA, Fig. 4e and f). Moreover, we tested the exogenous effect of itaconate on Nrf2 expression in IFN-γ-stimulated VSMCs. Interestingly, pretreatment with OI also enhanced Nrf2 expression and blocked IFN-γ-stimulated MMP9, MMP2 and MCP1 expression in VSMCs ($p<0.01$ vs. IFN-γ, Supplemental Fig. 5d), suggesting a regulatory role of itaconate in VSMC-mediated inflammation.

Nrf2 protein migration to cell nuclei is a crucial step for Nrf2 activation and function [42]. We treated Raw 264.7 macrophages with OI and observed that Nrf2 protein levels were significantly increased in the cytosol and nucleus ($p<0.01$, parametric unpaired t test, Fig. 4g), indicating that itaconate could promote Nrf2 nuclear translocation. In addition, OI increased the mRNA levels of known Nrf2-dependent genes, including Hmox1 and Nqo1, confirming that itaconate activated Nrf2 signaling (Supplemental Fig. 5e). Itaconate and its derivative OI have been demonstrated to alkylate Keap1 cysteine 151 (Cys151), dissociate the Keap1-Nrf2 complex, and stabilize and activate Nrf2 [34]. Based on these findings, we constructed a Cys151S mutant Keap1 vector. Raw 264.7 cells were transfected with the Cys151S mutant Keap1 vector ($Keap1^{C151S}$) or wild-type Keap1 vector ($Keap1^{WT}$). Western blotting showed that the OI-induced Nrf2 increase was blocked in cells with the Cys151S mutant Keap1 ($p<0.05$ vs. $Keap1^{WT}$+OI, Fig. 4h). These results indicated that alkylation of Keap1 Cys151S was the mechanism underlying itaconate-induced Nrf2 activation.

Subsequently, to study whether Nrf2 regulated inflammatory cytokine gene expression, we transfected Raw 264.7 macrophages with the Nrf2 overexpression plasmid (OE-Nrf2) or its negative control (NC) and then stimulated the cells with IFN-γ for 24 h. qPCR revealed that Nrf2 overexpression significantly inhibited INF-γ-induced IL-6 and IL-1β expression ($p<0.01$, parametric unpaired t test, Supplemental Fig. 6a). As Nrf2 is a transcription factor of many genes, we then used the Jaspar database (http://jaspar.binf.ku.dk/) to predict the binding sequence of Nrf2 (Fig. 4i). To assess the binding between Nrf2 and IL-6/IL-β, ChIP-qPCR analysis with an anti-Nrf2 antibody or anti-IgG antibody was performed and showed that Nrf2 bound to the promoter regions of IL-6 and IL-1β in macrophages (Fig. 4j). This indicated that Nrf2 inhibits the transcription of IL-6 and IL-1β through direct binding to the genes.

The preceding results indicated that itaconate suppressed IFN-γ-induced macrophage inflammatory responses by activating Nrf2.

3.5. Targeting Nrf2 affects Ang II-induced AAA formation

Since Nrf2 is a target molecule of itaconate, we performed gain- and loss-of-function studies to assess the role of Nrf2 in AAA formation.

The OE-Nrf2 and NC plasmids were generated and transfected into Raw 264.7 cells. qPCR assays confirmed the effectiveness of the

pretreated with OI or vehicle. Lamin B1 was tested as a marker of nuclear protein. $^{**}p<0.01$; n=5 per group (statistical analyses of Nrf2 protein expression between the control and OI groups in the cytosol or nucleus were performed using a parametric unpaired t test). (h) Nrf2 and Keap1 protein levels after transfection with the Cys151Ser mutant Keap1 ($Keap1^{C151S}$) or wild-type Keap1 ($Keap1^{WT}$). $^{**}p<0.01$, $^{*}p<0.05$; n=5 per group (parametric one-way ANOVA with post Bonferroni's multiple comparisons test). (i) The predicted binding sequence of Nrf2. (j) ChIP-qPCR using anti-Nrf2 or anti-IgG antibodies to assess the binding between Nrf2 and IL-6/IL-1β. $^{**}p<0.01$, n=3 per group (parametric unpaired t test).

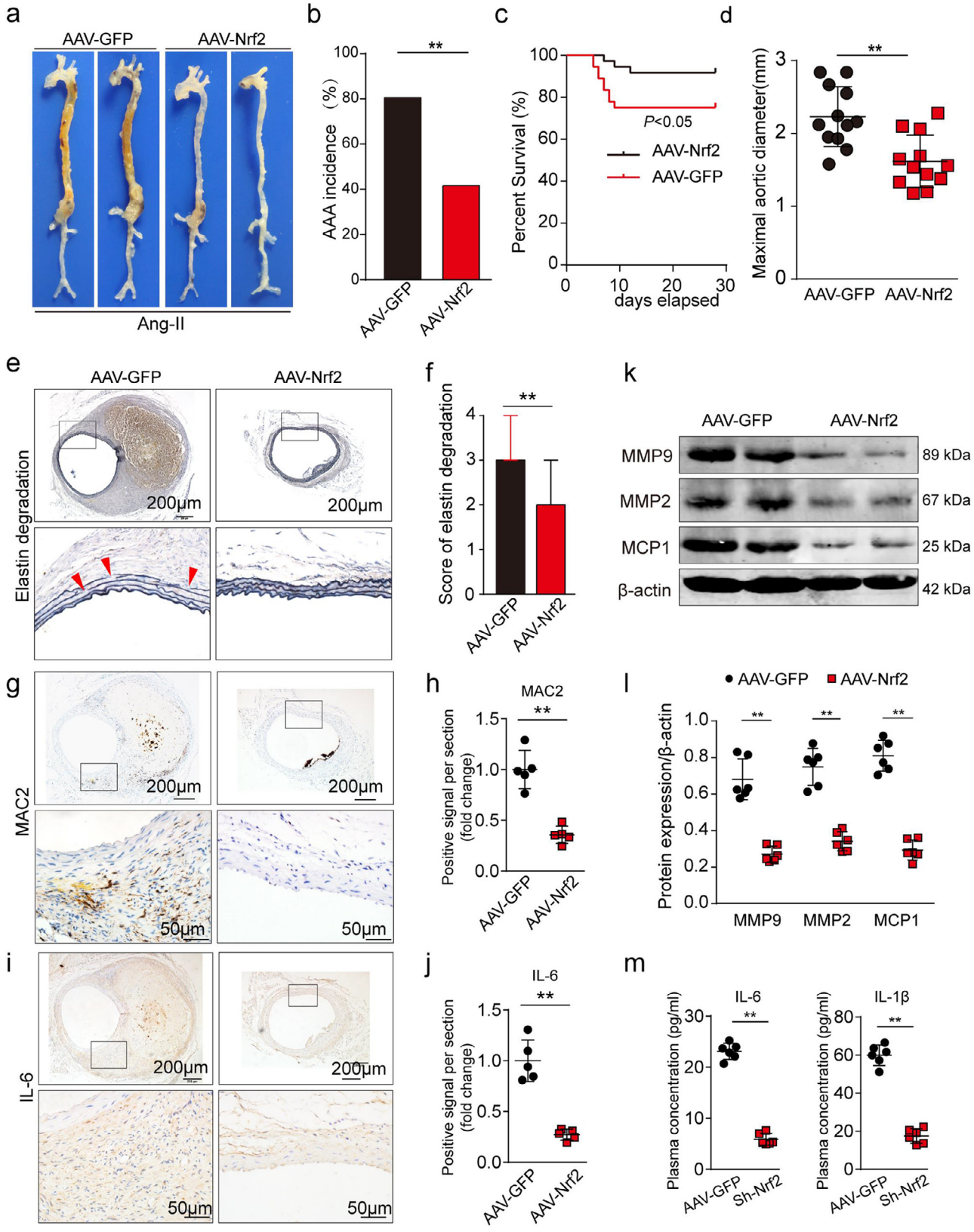

Fig. 5. Nrf2 overexpression protects against AAA formation in Ang II-treated Apoe$^{-/-}$ mice. (a) Representative images of the macroscopic features of AAA in the Ang II-infused Apoe$^{-/-}$ mice after transfection with AAV carrying an Nrf2 overexpression plasmid (AAV-Nrf2) or a control plasmid (AAV-GFP). (b) The incidence of Ang II-induced AAA in Apoe$^{-/-}$ mice. $^{**}p<0.01$ (Fisher's exact test). The number of mice that developed AAA included the deaths caused by abdominal aortic rupture. (c) The survival curve of Ang II-induced AAA in the two groups. $p<0.05$; n=36 per group (Log-rank (Mantel-Cox) test). (d) The maximal abdominal aortic diameter of the 28-day Ang II-infused Apoe$^{-/-}$ mice in the AAV-Nrf2 or AAV-GFP group. $^{**}p<0.01$; n=12 per group (parametric unpaired t test). (e and f) Representative staining with elastin and the elastin degradation score in the suprarenal aortas from Ang II-infused mice. The magnified photographs were taken at the location where the most severe elastin degradation occurred (scale bars=200 and 50 μm; magnified photographs). $^{**}p<0.01$; n=12 per group (non-parametric ANOVA Kruskal-Wallis test with post Dunn's multiple comparisons test). (g and h) Representative immunostaining and densitometric analysis of MAC2 in the suprarenal aortic walls (scale bars=200 and 50 μm). $^{**}p<0.01$; n=5 per group (parametric unpaired t test). (i and j) Representative immunostaining

overexpression plasmid (Supplemental Fig. 7a). Apoe$^{-/-}$ mice were injected with the AAV carrying the OE-Nrf2 plasmid (AAV-Nrf2 group) or its NC plasmid (AAV-GFP group). The overexpression effect of in vivo adenoviral gene transfer of Nrf2 was displayed by Western blotting (Supplemental Fig. 7b). Compared with AAV-GFP, Nrf2 protein was overexpressed after transfection with AAV-Nrf2 30 days after AAV transfection (Supplemental Fig. 8a). On the 30th day, mice were infused with Ang II to generate the AAA model as described above. Under baseline conditions, no difference in blood pressure was detected between the AAV-Nrf2 group and the AAV-GFP group (Supplemental Fig. 8b). Nrf2 overexpression attenuated AAA formation (Fig. 5a). The AAA incidence was lower in the AAV-Nrf2 group than in the AAV-GFP group (41.7% versus 80.6%) ($p<0.01$, Fisher's exact test, Fig. 5b). Aortic rupture mortality was lower in the AAV-Nrf2 group than in the AAV-GFP group (8.3% versus 25.0%) (Fig. 5c). Overexpression of Nrf2 decreased the maximal aortic diameter and elastin degradation score (Fig. 5d-f). Furthermore, overexpression of Nrf2 decreased infiltrating macrophages ($p<0.01$, parametric unpaired t test, Fig. 5g-h), as well as IL-6, MMP9, MMP2 and MCP1 expression in the aortic wall, as shown by immunohistochemistry staining (Fig. 5i-j, Supplemental Fig. 8c-f). Western blotting also showed decreased protein levels of MMP9, MMP2 and MCP1 in Nrf2-overexpressing mice ($p<0.01$, parametric unpaired t test, Fig. 5k-l). The inflammatory cytokines IL-6 and IL-1β in plasma were remarkably reduced in the AAV-Nrf2 group compared with the AAV-Nrf2 group ($p<0.01$, parametric unpaired t test, Fig. 5m). These results suggested that Nrf2 attenuated Ang II-induced mouse AAA formation.

In contrast, another AAV carrying the selected siRNA against Nrf2 (Sh-Nrf2) or scramble RNA (Scr-RNA) was administered to C57BL/6J mice, and successful Nrf2 knockdown was confirmed by Western blotting assays (Supplemental Fig. 7c-d). Nrf2 protein was inhibited in the Sh-Nrf2 group relative to the Scr-RNA group ($p<0.01$, parametric unpaired t test, Supplemental Fig. 9a). Then, the Ang II-induced model was generated on the 30th day as described previously. No difference was found in systolic blood pressure between the two groups during the 28-day Ang II infusion ($p>0.05$, parametric unpaired t test, Supplemental Fig. 9b). As expected, knockdown of Nrf2 increased AAA incidence and rupture mortality and significantly increased the maximal aortic diameter and elastin degradation score (Fig. 6a−f). And knockdown of Nrf2 specifically induced abdominal aortic dilation as no significant difference was found in the maximal ascending aortic diameter or thoracic aortic diameter ($p>0.05$, parametric unpaired t test, Supplemental Fig. 9c). Immunohistochemistry staining showed increased infiltrating macrophages and IL-6, MMP9, MMP2 and MCP1 expression throughout the vessel wall in Nrf2 knockdown mice compared with control mice (Fig. 6g−j, Supplemental Fig. 9d−g). Western blotting further confirmed the increased protein levels of MMP9, MMP2 and MCP1 in Nrf2 knockdown mice (Fig. 6k and l). Knockdown of Nrf2 also increased plasma IL-6 and IL-1β ($p<0.01$, parametric unpaired t test, Fig. 6m).

Taken together, these data confirmed that Nrf2 plays a protective role in AAA formation.

3.6. Exogenous addition of itaconate abolished AAA formation induced by overexpression of Keap1

To determine the role of the Nrf2 pathway in itaconate-mediated AAA protection, we used an AAV carrying the Keap1 overexpression plasmid to repress Nrf2 activity in vivo. Male C57BL/6J mice were randomized to three groups and separately transfected with control AAV-GFP or AAV-Keap1, or transfected with AAV-Keap1 and intraperitoneally injected with OI during AAA establishment. Consistent with our hypothesis, Keap1 overexpression promoted AAA formation, while addition of OI reversed this effect (Fig. 7a). Keap1 overexpression caused a 41.67% (15/36) AAA incidence and a 19.44% (7/36) aortic rupture mortality, compared with an 11.11% (4/36) incidence and zero mortality in control mice. OI supplementation caused a 13.89% (5/36) incidence and 2.78% (1/36) mortality compared with the AAV-Keap1 group (Fig. 7b and c). Additionally, in the AAV-Keap1 group, the maximal abdominal aortic diameter, the elastin degradation score were significantly higher than those of control mice, while the addition of OI lowered these indexes (Fig. 7d and f). At the same time, the maximal ascending diameter and thoracic diameter did not differ significantly among the three groups ($p>0.05$, parametric one-way ANOVA, Supplemental Fig. 10b). Besides, OI abrogated IL-6 and IL-1β production induced by overexpression of Keap1. ($p<0.01$ vs. AAV-Keap1, parametric one-way ANOVA, Supplemental Fig. 10c). Correspondingly, infiltrating macrophages and IL-6, MMP9, MMP2, and MCP1 expression were strongly increased in Keap1 overexpression mice as shown by immunohistochemistry staining, and these protein levels were significantly reduced in the OI addition group compared with the AAV-Keap1 group (Fig. 7g−j, Supplemental Fig. 10d-i).

These results further supported the notion that itaconate protects against AAA by regulating the Keap1/Nrf2 pathway.

4. Discussion

In the present study, we showed that itaconate, an endogenous metabolite, protected against AAA formation by inhibiting aortic inflammation without gene editing, while knockdown of Irg1 exhibited the opposite effect. Mechanistically, we revealed that itaconate inhibited vascular inflammation by enabling Nrf2 to inhibit the expression of downstream inflammatory genes via alkylation of Keap1. Furthermore, we found that knockdown of Nrf2 inhibited the protective effect of itaconate on aortic aneurysms. Our findings suggest that itaconate might be a safe and inexpensive therapeutic treatment for AAA.

In the current study, we fully demonstrated that itaconate significantly inhibited Ang II-induced AAA formation in Apoe$^{-/-}$ mice, as shown by inhibition of aortic enlargement and elastin degradation. Our results also demonstrated that itaconate reduced AAA by inhibiting aortic inflammation, as itaconate decreased the expression of the proinflammatory molecules IL-6 and IL-1β and decreased macrophage infiltration, all of which are major drivers of AAA formation and progression [3,43,44]. Lending support to our findings, studies have reported that itaconate contributes to the inactivation of inflammation in an ischemia-reperfusion injury model, in which itaconate enhanced IL-6 expression and IL-1β by controlling TCA cycle remodeling [20]. In addition to its role in Ang II-induced AAA in Apoe$^{-/-}$ mice, IRG1 deficiency markedly exacerbated the progression of Ang II-induced AAA in nonhyperlipidemic C57BL/6J mice. These results indicate that itaconate might be used against aortic aneurysm formation by suppressing vascular inflammation. The effectiveness, safety, and affordability of potential treatments are indispensable for clinical development. The characteristics of itaconate indicate that it has clinical therapeutic significance. Itaconate is an endogenous metabolite that can be processed into drugs for the treatment of aortic aneurysms without the aid of gene editing tools, indicating that itaconate might be a relatively safe drug because it avoids various limitations associated with gene editing, such as low gene transfer efficiency, immune responses, unpredictable insertional mutagenesis, and bioethics. Furthermore, unlike gene editing therapy, itaconate does not

and densitometric analysis of IL-6 in the suprarenal aortic walls (scale bars=200 and 50 μm). $^{**}p<0.01$; n=5 per group (parametric unpaired t test). (k and l) WB analysis of the protein levels of MMP2, MMP9, and MCP1 in the aortas from Ang II−infused Apoe$^{-/-}$ mice. $^{**}p<0.01$; n=6 per group (parametric unpaired t test). (m) Plasma IL-6 and IL-1β levels in the Ang II-treated Apoe$^{-/-}$ mice in the AAV-Nrf2 and AAV-GFP groups. $^{**}p<0.01$; n=6 per group (parametric unpaired t test).

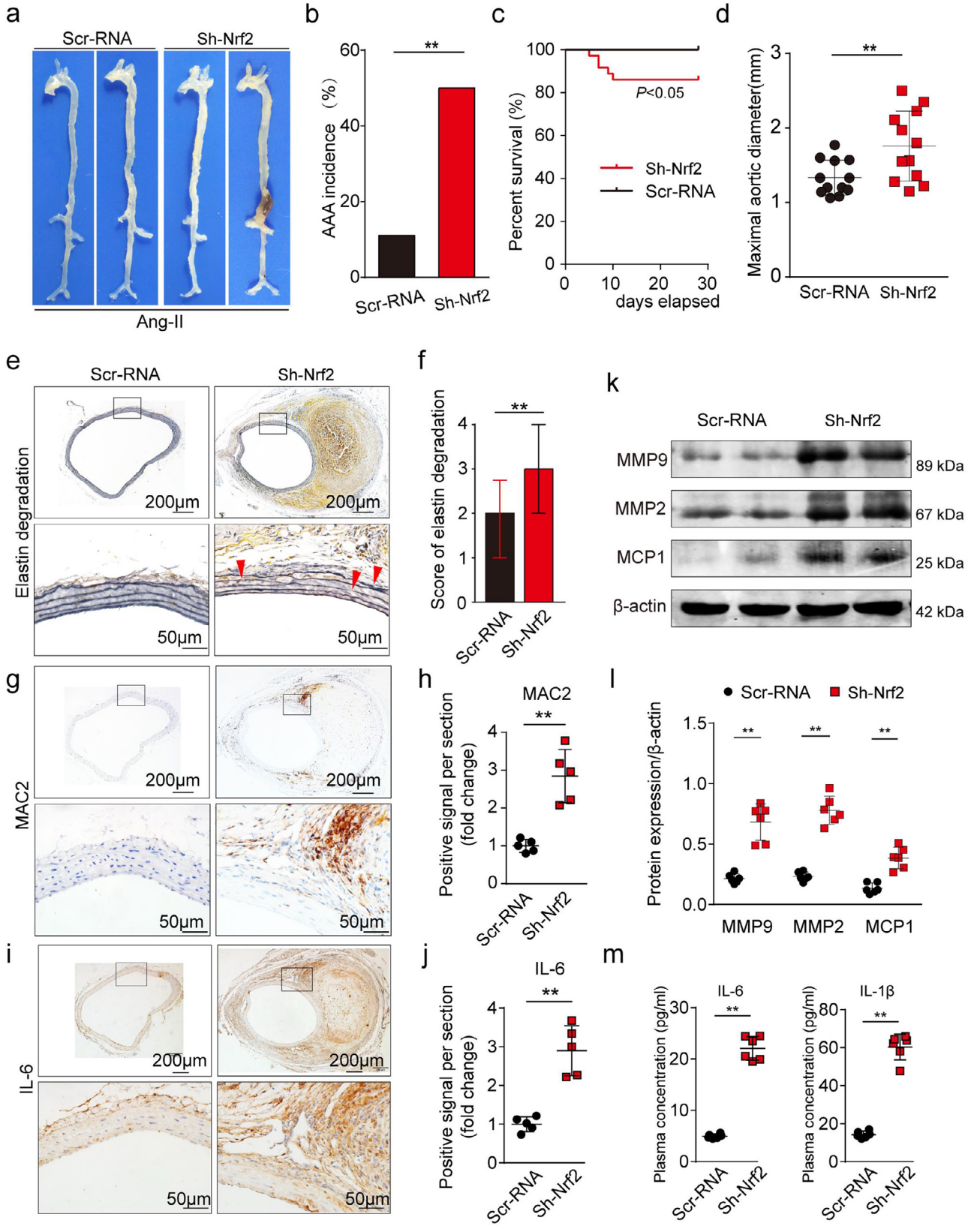

Fig. 6. Nrf2 reduction induces AAA formation in Ang II-treated C57/BL6J mice. (a) Representative images of the macroscopic features of AAA in the Ang II-infused C57BL/6J mice transfected with AAV carrying siRNA against Nrf2 (Sh-Nrf2) or scramble siRNA (Scr-RNA). (b) The incidence of Ang II-induced AAA in C57BL/6J mice. $^{**}p<0.01$ (Fisher's exact test). The number of mice that developed AAA included deaths caused by abdominal aortic rupture. (c) The survival curve of Ang II-induced AAA in the two groups. $p<0.05$; n=36 per group (Log-rank (Mantel-Cox) test). (d) The maximal abdominal aortic diameter in the Ang II−infused C57BL/6J mice. $^{**}p<0.01$; n=12 per group (parametric unpaired t test). (e and f) Representative staining with elastin and the elastin degradation score in the suprarenal aortas from Ang II−infused mice. The magnified photographs were taken at the location where the most severe elastin degradation occurred (scale bars=200 and 50 μm; magnified photographs). $^{**}p<0.01$; n=12 per group (non-parametric ANOVA Kruskal-Wallis test with post Dunn's multiple comparisons test). (g and h) Representative immunostaining and densitometric analysis of MAC2 in the suprarenal aortic walls (scale bars=200 and 50 μm). $^{**}p<0.01$; n=5 per group (parametric unpaired t test). (i and j) Representative immunostaining and densitometric analysis of IL-6 in the suprarenal aortic walls (scale bars=200 and 50 μm). $^{**}p<0.01$; n=5 per group (parametric unpaired t test). (k and l) WB analysis of the protein levels of MMP2, MMP9, and MCP1 in the aortas from Ang II−infused C57BL/6J mice. $^{**}p<0.01$; n=6 per group (parametric unpaired t test). (m) Plasma IL-6 and IL-1β levels in Ang II-treated C57BL/6J mice. $^{**}p<0.01$; n=6 per group (parametric unpaired t test).

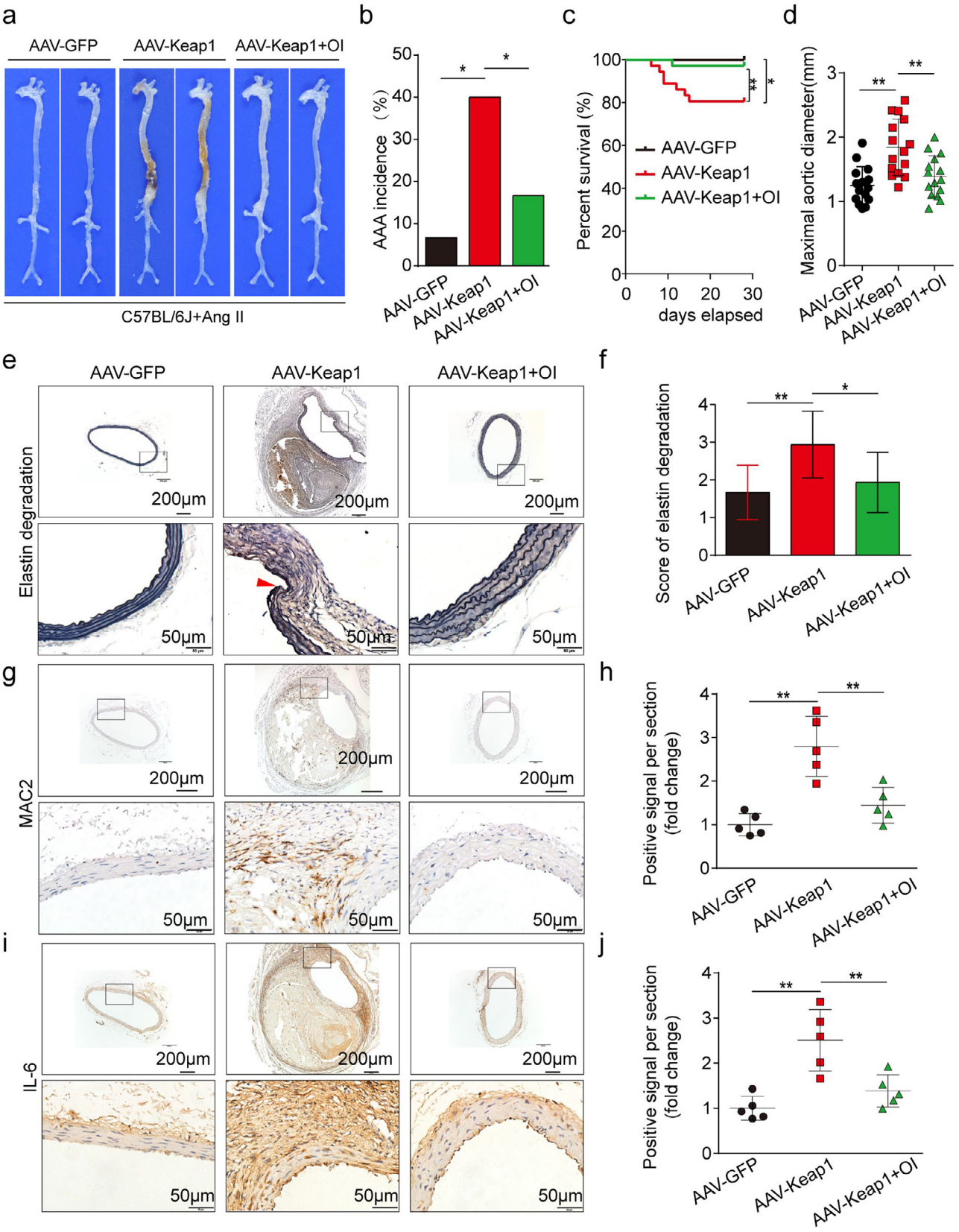

Fig. 7. Exogenous addition of OI abolished AAA formation induced by overexpression of Keap1 in Ang II-induced C57BL/6J mice. (a) Representative images of the macroscopic features of Ang II-induced AAA in the indicated group. (b) The incidence of Ang II-induced AAA in C57BL/6J mice. $^{*}p<0.05$; n=36 (Fisher's exact test). (c) The survival curve of Ang II-induced AAA in C57BL/6J mice. $^{**}p<0.01$, $^{*}p<0.05$; n=36 in each group (parametric one-way ANOVA with post Bonferroni's multiple comparisons test). (d) The maximal abdominal aortic diameter in Ang II−infused C57BL/6J mice. $^{*}p<0.05$; n=15 per group (parametric unpaired t test). (e and f) Representative staining with elastin and the elastin degradation score in the suprarenal aortas from Ang II−infused mice. The magnified photographs were taken at the location where the most severe elastin degradation occurred (scale bars= 200 and 50 μm; magnified photographs). $^{**}p<0.01$, $^{*}p<0.05$; n=15 per group (non-parametric ANOVA Kruskal-Wallis test with post Dunn's multiple comparisons test). (g and h) Representative immunostaining and densitometric analysis of MAC2 in the suprarenal aortic walls (scale bars=200 and 50 μm). $^{**}p<0.01$; n=5 per group (parametric unpaired t test). (i and j) Representative immunostaining and densitometric analysis of IL-6 in the suprarenal aortic walls (scale bars=200 and 50 μm). $^{**}p<0.01$; n=5 per group (parametric unpaired t test).

permanently affect genes and shows relatively flexible control of gene expression according to the actual clinical situation. More importantly, itaconate is readily available and can be produced in large quantities. Taken together, these findings suggest that itaconate might be a novel and inexpensive therapeutic treatment for AAA.

In biological process, some genes induced in response to stimulation have the ability to control the deleterious stimulation conversely. This kind of modulation is also considered as a self-protective strategy. Based on previous studies and our finding, itaconate, as an endogenous inflammation responsive metabolite, is highly upregulated under inflammatory stimuli and exerts a feedback anti-inflammation effect. However, when deleterious stimuli persists, the endogenous response may be insufficient to prevent the inflammatory disease, and therefore need to be augmented through exogenous addition. AAA is a chronic inflammatory disease. During the pathological process, persistent inflammatory reactions are beyond the regulatory capability of itaconate. Some similar examples are noted here. MicroRNA-21 is upregulated in AAA. Overexpression of miR-21 protects the aorta from further expansion and ultimate rupture [45]. Additionally, Nrf2, which is activated by oxidative stimuli, can restrain the aggravation of oxidative stress [46].

We further demonstrated that itaconate inhibited vascular inflammation by enabling Nrf2 to function as a transcriptional repressor of downstream inflammatory genes via alkylation of Keap1. Previous studies have shown that IFN-γ induces a strong upregulation of Irg1 in macrophages, which interrupts the Krebs cycle and promotes itaconate production [39,40]. During the AAA process, IFN-γ is elevated in both tissues and blood, which activates macrophages and induces MMP production [37,38]. Therefore, in our in vitro experiments, we induced macrophages with IFN-γ to mimic the AAA environment. Nrf2, a transcription factor, is an important negative regulator of inflammatory responses [47,48]. In our study, in Raw264.7 cells, itaconate promoted the activation and expression of Nrf2 and inhibited the expression of IL-6, IL-1β, MMP9 and MCP1 induced by IFN-γ, which aggravated the formation of AAA by increasing aortic inflammation [49]. Moreover, we isolated peritoneal macrophages from Ang II-treated Apoe$^{-/-}$ mice, which were treated with DMSO or itaconate. We also found that itaconate significantly enhanced the activation and expression of Nrf2 and inhibited the expression of related inflammatory factors in peritoneal macrophages, while Irg1 knockdown exhibited the opposite results. These findings indicated that itaconate inhibited aortic inflammatory activation by increasing the activation and expression of Nrf2. Furthermore, we demonstrated that itaconate activated Nrf2 via alkylation of Keap1. Previous studies have shown that the alkylation of Keap1 is the key to activating Nrf2 [34]. We found that a mutant of Keap1 alkylation sites significantly inhibited itaconate-induced Nrf2 activation. In addition, we explored the mechanism underlying Nrf2-mediated inhibition of IL-6 and IL-1β. A previous study showed that Nrf2 might function as a transcriptional repressor of inflammatory genes [50]. In our study, the bioinformatic tools showed that Nrf2 binds to a few binding sites in the IL-6 and IL-1β promoter regions. The ChIP results showed that Nrf2 can effectively bind to the IL-6 and IL-1β promoter regions in Raw 264.7 cells, indicating that Nrf2 might function as a transcriptional repressor of IL-6 and IL-1β. Taken together, our results confirmed that itaconate inhibited AAA formation by enabling Nrf2 to function as a transcriptional repressor of IL-6 and IL-1β via alkylation of Keap1.

We further demonstrated that Nrf2 is indispensable for the protective effect of itaconate on aortic aneurysms through rescue experiments. Our results showed that Nrf2 knockdown aggravated AAA formation, upregulated the expression of IL-6, IL-1β, MMPs and MCP1 and increased macrophage infiltration and that Nrf2 overexpression exerted protective effects. These in vivo results demonstrated that Nrf2 protects against AAA formation. Furthermore, in rescue experiments, we found that itaconate significantly inhibited Ang II-induced AAA formation, reduced AAA and decreased the expression of proinflammatory molecules in Ang II-infused Apoe$^{-/-}$ mice, and these effects were inhibited by Nrf2 deficiency. In summary, our findings revealed that Nrf2 is essential for the protective effect of itaconate on aortic aneurysms and that the itaconate/Keap1/Nrf2 pathway plays a critical role in AAA formation.

There are some limitations of our study. Although mouse macrophage-specific knockout of Irg1 or Nrf2 is an ideal animal model when investigating the role of Irg1 or Nrf2 in AAA, we used AAV2-mediated Irg1 or Nrf2 suppression in mouse macrophages. Previous studies have demonstrated that mouse macrophages are easily transfected by AAV2 [26], while arterial SMCs are easily transfected by AAV9 rather than AAV2 [51]. Second, our study focused on the itaconate/Keap1/Nrf2 pathway in AAA; however, as itaconate may potentially regulate multiple signaling pathways in different cells, whether there are other potential downstream signaling pathways of itaconate remains to be investigated. In spite of the other potential downstream signaling pathways of itaconate, we demonstrated that Nrf2 is essential for the protective effect of itaconate on aortic aneurysms.

In summary, our work showed that Irg1/itaconate protected against AAA formation by promoting the expression and activation of Nrf2, which suppressed AAA formation by inhibiting the expression of downstream inflammatory genes. Our findings suggest the potential of Irg1/itaconate to serve as a novel and inexpensive therapeutic target for AAA.

Declaration of Competing Interest

None.

Acknowledgments

We thank Xiangshi Li for his technical help.

Funding sources

This work was supported by grants to Jianping Bin from the National Natural Science Foundation of China (No. 81771857, 81571698) and Guangzhou Regenerative Medicine and Health Laboratory of Guangdong (2018GZR110105009). The funders had no role in the study design, data collection, data analysis, interpretation, and writing of the report.

Author contributions

The contribution of each author is as follows: Haoyu Song wrote the paper, performed the experiments and analyzed the data, Hao Zheng, Tong Xu, Xiaofei Feng, Yanxian Lai and Guoquan Wei performed the experiments and analyzed the data, Yang Yang and Xiang He analyzed the data and wrote the paper, Wangjun Liao and Yulin Liao designed the research, and Lintao Zhong and Jianping Bin designed the research and wrote the paper.

Supplementary materials

Supplementary material associated with this article can be found in the online version at doi:10.1016/j.ebiom.2020.102832.

References

[1] Wang Y, Ait-Oufella H, Herbin O, et al. TGF-beta activity protects against inflammatory aortic aneurysm progression and complications in angiotensin II-infused mice. J Clin Investigat 2010;120(2):422–32.

[2] Ijaz T, Sun H, Pinchuk IV, Milewicz DM, Tilton RG, Brasier AR. Deletion of NF-kappaB/RelA in Angiotensin II-sensitive mesenchymal cells blocks aortic vascular inflammation and abdominal aortic aneurysm formation. Arterioscl Thromb Vascul Biol 2017;37(10):1881–90.

[3] Isoda K, Akita K, Kitamura K, et al. Inhibition of interleukin-1 suppresses angiotensin II-induced aortic inflammation and aneurysm formation. Int J Cardiol 2018;270:221–7.
[4] Johnston WF, Salmon M, Su G, et al. Genetic and pharmacologic disruption of interleukin-1beta signaling inhibits experimental aortic aneurysm formation. Arterioscl Thromb Vascular Biol 2013;33(2):294–304.
[5] Chen HZ, Wang F, Gao P, et al. Age-Associated Sirtuin 1 reduction in vascular smooth muscle links vascular senescence and inflammation to abdominal aortic aneurysm. Circ Res 2016;119(10):1076–88.
[6] Maegdefessel L, Spin JM, Raaz U, et al. miR-24 limits aortic vascular inflammation and murine abdominal aneurysm development. Nature Commun 2014;5:5214.
[7] Sun Y, Zhong L, He X, et al. LncRNA H19 promotes vascular inflammation and abdominal aortic aneurysm formation by functioning as a competing endogenous RNA. J Molecular Cellular Cardiol 2019;131:66–81.
[8] Dale MA, Xiong W, Carson JS, et al. Elastin-Derived peptides promote abdominal aortic aneurysm formation by modulating M1/M2 Macrophage Polarization. J Immunol 2016;196(11):4536–43.
[9] Nishihara M, Aoki H, Ohno S, et al. The role of IL-6 in pathogenesis of abdominal aortic aneurysm in mice. Plos One 2017;12(10):e0185923.
[10] Harada S, Takebayashi T, Kurihara A, et al. Metabolomic profiling reveals novel biomarkers of alcohol intake and alcohol-induced liver injury in community-dwelling men. Environ Health Prevent Med 2016;21(1):18–26.
[11] Wang B, Zeng H, Wen Z, Chen C, Wang DW. CYP2J2 and its metabolites (epoxyeicosatrienoic acids) attenuate cardiac hypertrophy by activating AMPKalpha2 and enhancing nuclear translocation of Akt1. Aging Cell 2016;15(5):940–52.
[12] Khatua TN, Borkar RM, Mohammed SA, Dinda AK, Srinivas R, Banerjee SK. Novel Sulfur Metabolites of Garlic Attenuate Cardiac Hypertrophy and Remodeling through Induction of Na(+)/K(+)-ATPase Expression. Front Pharmacol 2017;8:18.
[13] Althurwi HN, Maayah ZH, Elshenawy OH, El-Kadi AO. Early Changes in Cytochrome P450s and Their Associated Arachidonic Acid Metabolites Play a Crucial Role in the Initiation of Cardiac Hypertrophy Induced by Isoproterenol. Drug Metabolism Dispos Biolog Fate Chem 2015;43(8):1254–66.
[14] Elkhatali S, El-Sherbeni AA, Elshenawy OH, Abdelhamid G, El-Kadi AO. 19-Hydroxyeicosatetraenoic acid and isoniazid protect against angiotensin II-induced cardiac hypertrophy. Toxicol Appl Pharmacol 2015;289(3):550–9.
[15] Cason CA, Dolan KT, Sharma G, et al. Plasma microbiome-modulated indole- and phenyl-derived metabolites associate with advanced atherosclerosis and postoperative outcomes. J Vascular Surg 2018;68(5):1552–62 e7.
[16] Wang Z, Klipfell E, Bennett BJ, et al. Gut flora metabolism of phosphatidylcholine promotes cardiovascular disease. Nature 2011;472(7341):57–63.
[17] Ross S, Eikelboom J, Anand SS, et al. Association of cyclooxygenase-2 genetic variant with cardiovascular disease. Eur Heart J 2014;35(33) 2242-8a.
[18] Zhang L, Ovchinnikova O, Jonsson A, et al. The tryptophan metabolite 3-hydroxyanthranilic acid lowers plasma lipids and decreases atherosclerosis in hypercholesterolaemic mice. Eur Heart J 2012;33(16):2025–34.
[19] Thomas SC, Alhasawi A, Appanna VP, Auger C, Appanna VD. Brain metabolism and Alzheimer's disease: the prospect of a metabolite-based therapy. J Nutrit, Health Aging 2015;19(1):58–63.
[20] Lampropoulou V, Sergushichev A, Bambouskova M, et al. Itaconate Links Inhibition of Succinate Dehydrogenase with Macrophage Metabolic Remodeling and Regulation of Inflammation. Cell Metab 2016;24(1):158–66.
[21] Bambouskova M, Gorvel L, Lampropoulou V, et al. Electrophilic properties of itaconate and derivatives regulate the IkappaBzeta-ATF3 inflammatory axis. Nature 2018;556(7702):501–4.
[22] Yu XH, Zhang DW, Zheng XL, Tang CK. Itaconate: an emerging determinant of inflammation in activated macrophages. Immunol Cell Biol 2019;97(2):134–41.
[23] Zhong L, He X, Si X, et al. SM22alpha (Smooth Muscle 22alpha) Prevents Aortic Aneurysm Formation by Inhibiting Smooth Muscle Cell Phenotypic Switching Through Suppressing Reactive Oxygen Species/NF-kappaB (Nuclear Factor-kappaB). Arterioscl Thromb Vascular Biol 2019;39(1):e10–25.
[24] Li L, Zhang HN, Chen HZ, et al. SIRT1 Acts as a Modulator of Neointima Formation Following Vascular Injury in Mice. Circ Res 2011;108(10) 1180-U95.
[25] Guo SC, Shen SX, Wang JF, et al. Detection of High-Risk Atherosclerotic Plaques with Ultrasound Molecular Imaging of Glycoprotein IIb/IIIa Receptor on Activated Platelets. Theranostics 2015;5(4):418–30.
[26] Fu Y, Gao C, Liang Y, et al. Shift of Macrophage Phenotype Due to Cartilage Oligomeric Matrix Protein Deficiency Drives Atherosclerotic Calcification. Circ Res 2016;119(2):261–76.
[27] Li HR, Lu YK, Sun YL, et al. Diagnostic Ultrasound and Microbubbles Treatment Improves Outcomes of Coronary No-Reflow in Canine Models by Sonothrombolysis. Crit Care Med 2018;46(9):E912–E20.
[28] Lai YX, Li JY, Zhong LT, et al. The pseudogene PTENP1 regulates smooth muscle cells as a competing endogenous RNA. Clin Sci 2019;133(13):1439–55.
[29] Zhang W, Zhang Y, Guo X, et al. Sirt1 Protects Endothelial Cells against LPS-Induced Barrier Dysfunction. Oxidat Med Cellular Long 2017;2017:4082102.
[30] Quintana RA, Taylor WR. Cellular Mechanisms of Aortic Aneurysm Formation. Circ Res 2019;124(4):607–18.
[31] Kim CW, Kumar S, Son DJ, Jang IH, Griendling KK, Jo H. Prevention of abdominal aortic aneurysm by anti-microRNA-712 or anti-microRNA-205 in angiotensin II-infused mice. Arterioscl Thromb Vascular Biol 2014;34(7):1412–21.
[32] Daugherty A, Cassis LA. Mouse models of abdominal aortic aneurysms. Arterioscl Thromb Vascular Biol 2004;24(3):429–34.
[33] Cassis LA, Gupte M, Thayer S, et al. ANG II infusion promotes abdominal aortic aneurysms independent of increased blood pressure in hypercholesterolemic mice. Am J Physiol Heart Circul Physiol 2009;296(5) H1660-5.
[34] Mills EL, Ryan DG, Prag HA, et al. Itaconate is an anti-inflammatory metabolite that activates Nrf2 via alkylation of KEAP1. Nature 2018;556(7699) 113-+.
[35] Longo GM, Xiong W, Greiner TC, Zhao Y, Fiotti N, Baxter BT. Matrix metalloproteinases 2 and 9 work in concert to produce aortic aneurysms. J Clinical Invest 2002;110(5):625–32.
[36] Trivedi DB, Loftin CD, Clark J, et al. beta-Arrestin-2 deficiency attenuates abdominal aortic aneurysm formation in mice. Circ Res 2013;112(9):1219–29.
[37] Wang Q, Ding Y, Song P, et al. Tryptophan-derived 3-hydroxyanthranilic acid contributes to angiotensin ii-induced abdominal aortic aneurysm formation in mice in vivo. Circulation 2017;136(23):2271–83.
[38] Xiong W, Zhao Y, Prall A, Greiner TC, Baxter BT. Key roles of CD4+ T cells and IFN-gamma in the development of abdominal aortic aneurysms in a murine model. J Immunol 2004;172(4) 2607-12.
[39] Naujoks J, Tabeling C, Dill BD, et al. IFNs Modify the Proteome of Legionella-Containing Vacuoles and Restrict Infection Via IRG1-Derived Itaconic Acid. PLoS Pathogens 2016;12(2):e1005408.
[40] Michelucci A, Cordes T, Ghelfi J, et al. Immune-responsive gene 1 protein links metabolism to immunity by catalyzing itaconic acid production. Proc Natl Acad Sci USA 2013;110(19):7820–5.
[41] Wang KC, Li YH, Shi GY, et al. Membrane-Bound Thrombomodulin Regulates Macrophage Inflammation in Abdominal Aortic Aneurysm. Arterioscler Thromb Vascular Biol 2015;35(11):2412–22.
[42] Hayes JD, Dinkova-Kostova AT. The Nrf2 regulatory network provides an interface between redox and intermediary metabolism. Trends Biochem Sci 2014;39(4):199–218.
[43] Jones KG, Brull DJ, Brown LC, et al. Interleukin-6 (IL-6) and the prognosis of abdominal aortic aneurysms. Circulation 2001;103(18):2260–5.
[44] Tieu BC, Lee C, Sun H, et al. An adventitial IL-6/MCP1 amplification loop accelerates macrophage-mediated vascular inflammation leading to aortic dissection in mice. The Journal of clinical investigation 2009;119(12):3637–51.
[45] Maegdefessel L, Azuma J, Toh R, et al. MicroRNA-21 blocks abdominal aortic aneurysm development and nicotine-augmented expansion. Sci Transl Med 2012;4(122) 122ra22.
[46] Thimmulappa RK, Lee H, Rangasamy T, et al. Nrf2 is a critical regulator of the innate immune response and survival during experimental sepsis. J Clin Invest 2006;116(4):984–95.
[47] Ahmed SM, Luo L, Namani A, Wang XJ, Tang X. Nrf2 signaling pathway: Pivotal roles in inflammation. Biochim et Biophys Acta Molecular Basis Disease 2017;1863(2):585–97.
[48] Mohan S, Gupta D. Crosstalk of toll-like receptors signaling and Nrf2 pathway for regulation of inflammation. Biomed Pharmacoth 2018;108:1866–78.
[49] Shimizu K, Mitchell RN, Libby P. Inflammation and cellular immune responses in abdominal aortic aneurysms. Arterioscl Thromb Vascular Biol 2006;26(5):987–94.
[50] Kobayashi EH, Suzuki T, Funayama R, et al. Nrf2 suppresses macrophage inflammatory response by blocking proinflammatory cytokine transcription. Nature Commun 2016;7:11624.
[51] Bostick B, Ghosh A, Yue Y, Long C, Duan D. Systemic AAV-9 transduction in mice is influenced by animal age but not by the route of administration. Gene Therapy 2007;14(22):1605–9.